



1 Quantifying the Impacts of Marine Aerosols over the Southeast 2 Atlantic Ocean using a chemical transport model: Implications 3 for aerosol-cloud interactions

4 Mashiat Hossain¹, Rebecca M. Garland², Hannah M. Horowitz¹

5 ¹ Civil and Environmental Engineering, University of Illinois Urbana-Champaign, IL, USA

6 ² Department of Geography, Geoinformatics and Meteorology, University of Pretoria, Pretoria, South Africa

7 *Correspondence to:* Mashiat Hossain (mashiat3@illinois.edu), Hannah M. Horowitz (hmhorow@illinois.edu)

8 **Abstract.** The southeast Atlantic region, characterized by persistent stratocumulus clouds, has one of the highest
9 uncertainties in aerosol radiative forcing and significant variability across climate models. In this study, we analyze
10 the seasonally varying role of marine aerosol sources and identify key uncertainties in aerosol composition at cloud-
11 relevant altitudes over the southeast Atlantic using the GEOS-Chem chemical transport model. We evaluate simulated
12 aerosol optical depth (AOD) and speciated aerosol concentrations against those collected from ground observations
13 and aircraft campaigns such as LASIC, ORACLES, and CLARIFY, conducted during 2017. The model consistently
14 underestimates AOD relative to AERONET, particularly at remote locations like Ascension Island. However, when
15 compared with aerosol mass concentrations from aircraft campaigns during the biomass burning period, it performs
16 adequately at cloud-relevant altitudes, with a normalized mean bias (NMB) between -3.5% (CLARIFY) and -7.5%
17 (ORACLES). At these altitudes, organic aerosols (63%) dominate during the biomass burning period, while sulfate
18 (41%) prevails during austral summer, when dimethylsulfide (DMS) emissions peak in the model. Our findings
19 indicate that marine sulfate can account for up to 69% of total sulfate during high DMS period. Sensitivity analyses
20 indicate that refining DMS emissions and oxidation chemistry may increase sulfate aerosol produced from marine
21 sources, highlighting their overall importance. Additionally, we find marine primary organic aerosol emissions may
22 substantially increase total organic aerosol concentrations, particularly during austral summer. This study underscores
23 the imperative need to refine marine emissions and their chemical transformations to better predict aerosol-cloud
24 interactions and reduce uncertainties in aerosol radiative forcing over the southeast Atlantic.

25 1 Introduction

26 Marine aerosols are a primary contributor to natural atmospheric aerosols, and consequently influence the Earth's
27 radiative balance (Spracklen et al., 2008; Vignati et al., 2001). Aerosols in the marine boundary layer have significant
28 impact on the properties of low-altitude marine clouds, particularly their ability to reflect solar radiation and cool the
29 climate (Seinfeld and Pandis, 2016; Wood, 2012; Chen et al., 2014; Quinn et al., 2017). The southeast Atlantic (SEA)
30 is marked by a persistent deck of low-level stratocumulus (Sc) clouds. However, aerosol radiative forcing in the region
31 exhibits highest uncertainty and one of the largest intermodel spread, primarily due to the differences in modeled cloud
32 fraction (Stier et al., 2013; Zuidema et al., 2016), as well as aerosol and cloud properties (Doherty et al., 2022). These
33 uncertainties are further compounded by poorly constrained optical properties of the absorbing biomass burning



34 aerosols, the vertical distribution of aerosols relative to these clouds and the interaction of aerosols with marine
35 boundary layer clouds (Zuidema et al., 2016), and limited observations of aerosols and their precursors in remote
36 marine environments (Croft et al., 2021). In this study, we investigate the role of marine aerosols and sources of
37 uncertainty affecting aerosol composition in this critical region of aerosol-cloud interactions over the SEA.

38 The SEA region encompasses the Benguela upwelling system (BUS), renowned for its high primary production of
39 marine phytoplankton and fish populations (Shannon and Nelson, 1996; Jarre et al., 2015). This elevated
40 phytoplankton activity serves as the main natural source of the volatile organic compound dimethylsulfide (DMS),
41 thereby influencing the global tropospheric sulfur budget (Andreae, 1990; Bates et al., 1992). Once released into the
42 atmosphere through air-sea exchange, DMS undergoes complex chemical transformations. In the gas phase, it is
43 oxidized to form H_2SO_4 and methanesulfonic acid (MSA), which has implications for new particle formation (Chen
44 et al., 2015); while in the aqueous phase, it leads to the production of MSA and sulfate aerosols, impacting cloud
45 microphysical properties (Kaufman and Tanré, 1994). Despite its significance, the exact mechanisms of DMS
46 oxidation and subsequent formation of sulfate and MSA remain inadequately understood (Ravishankara et al., 1997;
47 Barnes et al., 2006; Hoffmann et al., 2016), leading to largest uncertainty of aerosol radiative forcing within climate
48 models (Carslaw et al., 2013). Additionally, marine aerosols comprise primary aerosols such as sea spray aerosols,
49 which consist of sea salt and organic matter, released into the atmosphere primarily by the bubble-bursting process
50 (O'Dowd and De Leeuw, 2007; Russell et al., 2010; Prather et al., 2013; Brooks and Thornton, 2018). Investigating
51 the uncertainties related to marine emissions and chemistry are crucial to refine our understanding of the impacts of
52 marine aerosols on climate.

53 The SEA lies at the confluence of not only marine aerosols, but other natural and anthropogenic aerosols from local
54 and distant origin (Andreae et al., 1995; Swap et al., 1996; Formenti et al., 1999; Swap et al., 2003; Tournadre, 2014).
55 During the austral spring (August to October), seasonal fires in the neighboring southern African region contribute
56 nearly one-third of global total biomass burning emissions (van der Werf et al., 2010). This seasonal influx of biomass
57 burning aerosols aloft interacts with the underlying Sc deck, introducing considerable variability into aerosol forcing
58 assessments in the SEA region (Lindesay et al., 1996; Swap et al., 2003). To address these uncertainties, several
59 international field campaigns were conducted between 1992 and 2018 during the peak biomass burning season (Swap
60 et al., 2003; Formenti et al., 2019; Haywood et al., 2021; Redemann et al., 2021). Despite the region being a prolific
61 source of marine aerosols throughout the year, the potential impact of aerosols on regional climate dynamics through
62 interactions with the persistent low-level marine clouds outside of the biomass burning season has been largely
63 overlooked.

64 Here, we use the GEOS-Chem global chemical transport model to analyze high-resolution, seasonally varying aerosol
65 composition at the altitudes of persistent stratocumulus clouds over the SEA. We specifically focus on the role of
66 marine aerosols, analyzing their contributions to sulfate and organic aerosol concentrations. We evaluate simulated
67 aerosol optical depth (AOD) and speciated aerosol concentrations against observational data from the Aerosol Robotic
68 Network (AERONET) and the Layered Atlantic Smoke Interactions with Clouds (LASIC), ObseRvations of Aerosols



69 above CLOUDS and their intERactionS (ORACLES), and CLOUD–Aerosol–Radiation Interaction and Forcing
70 (CLARIFY) field campaigns during the year 2017. We assess the sensitivity of our results to uncertainty in DMS
71 oxidation mechanisms and emissions of DMS, SO₂, and marine primary organics. Our findings aim to enhance
72 understanding of the seasonally varying role of marine aerosols in aerosol-cloud interactions in the SEA by a
73 comprehensive evaluation of aerosol composition at cloud altitudes.

74 **2 Methodology**

75 **2.1 Model Description**

76 Here, we use the GEOS-Chem 3D atmospheric chemical transport model version 13.3.3 with detailed gas- and aerosol-
77 phase tropospheric chemistry (<https://zenodo.org/records/5748260>). The model is driven by meteorology from the
78 Modern-Era Retrospective Analysis for Research and Applications, Version-2 (MERRA2) reanalysis, from the NASA
79 Global Modeling Assimilation Office (GMAO) (Gelaro et al., 2017). We perform nested grid simulations over the
80 southwestern coast of Africa (40°W–20°E, 0–40°S) with a horizontal resolution of 0.5° by 0.625° and extending over
81 47 vertical layers from the surface to 0.01hPa. A chemical time step of 20 minutes and transport time step as 10
82 minutes is applied, as recommended by Philip et al. (2016). Prior to the target year, 2017, we conduct a 6-month spin-
83 up simulation. Boundary conditions are obtained from global simulations performed at 4° latitude × 5° longitude
84 horizontal resolution for the same year after a 6-month initialization.

85 In GEOS-Chem, carbonaceous aerosol includes organic aerosols (OA) and black carbon (BC). BC follows Park et al.
86 (2003) and Wang et al. (2014). Organic aerosol follows the “simple” scheme which treats primary organic aerosol
87 (POA) as non-volatile and includes irreversible direct yield of SOA from precursors (Pai et al., 2020). Sulfate
88 (Alexander et al., 2009), nitrate (Jaeglé et al., 2018), and ammonium (Fountoukis and Nenes, 2007) thermodynamic
89 partitioning is estimated using the ISORROPIA II thermodynamic model (Fountoukis and Nenes, 2007). Monthly
90 anthropogenic emissions follow the Community Emissions Data System (CEDSV2) inventory (Hoesly et al., 2018).
91 Biomass burning emissions are calculated using the Global Fire Emissions Database (GFED4.1s) at 0.25°×0.25°
92 spatial resolution, with fractional daily and 3-hourly scaling factors applied to the cumulative monthly data (van der
93 Werf et al., 2017). DMS emissions in the standard model use the Lana et al. (2011) climatology, which compiles DMS
94 concentrations using data from the Global Surface Seawater DMS Database (<http://saga.pmel.noaa.gov/dms/>)
95 collected from 1972 to 2009, incorporated with additional observations from the South Pacific (Lee et al., 2010). The
96 standard DMS oxidation mechanism in the model includes only three gas-phase DMS reactions, which directly yield
97 SO₂ and MSA according to the reaction mechanism outlined by Chin et al. (1996), and incorporates updated reaction
98 rate coefficients from Burkholder et al. (2015). Sea-salt aerosol (SSA) emissions from the open ocean are sea surface
99 temperature-dependent (Jaeglé et al., 2011). Dust emissions include natural dust (Fairlie et al., 2007) and
100 anthropogenic dust from the AFCID inventory (Philip et al., 2017).

101 In this study, we carry out multiple simulations to explore the sensitivity of marine aerosols to various emission
102 sources. To quantify the impact of marine sources on sulfate aerosols within the stratocumulus cloud layer, we perform



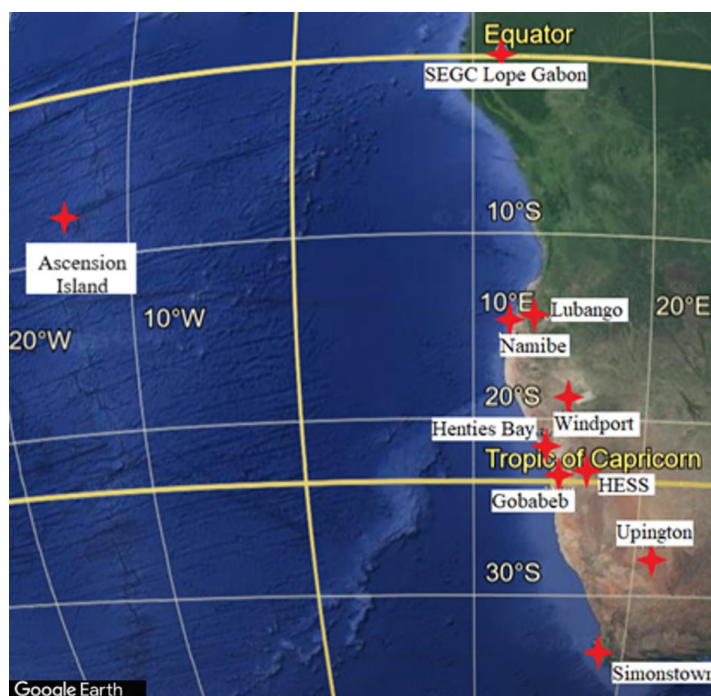
103 a high-resolution ($0.5^\circ \times 0.625^\circ$) marine emissions only sensitivity simulation where SO_2 and SO_4 emissions from
104 anthropogenic sources, biomass burning, volcanic activity, ships and aviation were turned off. Additionally, to
105 investigate the sensitivity of DMS emission fluxes to surface ocean DMS concentrations, we perform an additional
106 simulation with DMS concentrations from Galí et al. (2018). In this dataset, DMS concentrations are estimated through
107 a remote-sensing algorithm that integrates satellite-derived estimates of chlorophyll and light penetration, along with
108 climatological mixed layer depth (Galí et al., 2018). Furthermore, we assess the impact of adding marine POA, co-
109 emitted with sea-salt aerosols (Gantt et al., 2015), on the overall organic aerosol burden, which is not included in the
110 standard model configuration. Finally, to evaluate how uncertainty in biomass burning SO_2 emissions affects the
111 relative importance of marine emissions to sulfate aerosol, we conduct two sets of sensitivity simulations using the
112 Quick Fire Emissions Dataset (QFED) (Darrenov & da Silva, 2013; Das et al., 2017), and the Global Fire
113 Assimilation System (GFAS) (Kaiser et al., 2012; Su et al., 2023). Each of these inventories differ in data sources,
114 methodology, temporal resolution and plume injection height. These sensitivity analyses were conducted for the year
115 2017, following a six-month spin-up period. Details regarding the spatial resolution used in each sensitivity analysis
116 are provided in Table A1.

117 2.2 Ground-based measurements

118 We evaluate simulated aerosol optical depth (AOD) against AOD retrieved from the ground-based Aerosol Robotic
119 Network (AERONET) of sun photometers with direct sun measurements every 15 min (Holben et al., 1998). We use
120 Level 2.0 Version 3 data that have improved cloud screening algorithms (Giles et al., 2019). We strategically select
121 nine sites in the study domain along coastal and oceanic regions, as shown in Fig. 1. Site information, including the
122 coordinates, number of months with available data and the average daily AOD, is summarized in Table A2. The
123 AERONET monthly average AOD is computed from daily averages for sites with at least 3 months of observations
124 during the model simulation period (year 2017) and months with at least 15 days of measurements. These are then
125 compared with the monthly mean AOD from the GEOS-Chem model.

126 The modeled AOD is computed at 550 nm wavelength by vertically integrating scattering and absorption coefficients
127 based on the properties of various aerosol components, such as size distributions, hygroscopicity, refractive indices,
128 and densities (Latimer and Martin, 2019). For comparison with modeled monthly AOD, daily measurements at each
129 site at 440 nm are first interpolated to the standard wavelength of 550 nm using the local Ångström exponent between
130 440 and 870 nm channels, following the Ångström power law (Eq. (1); Martínez-Lozano et al., 1998). These
131 interpolated values are then averaged to calculate the observed mean monthly AOD. The interpolation formula used
132 is:

$$133 \quad AOD_{(550\text{nm})} = AOD_{(440\text{nm})} * \left(\frac{550}{440}\right)^{-\alpha \text{ext}\left(\frac{440}{870}\right)} \quad (1)$$



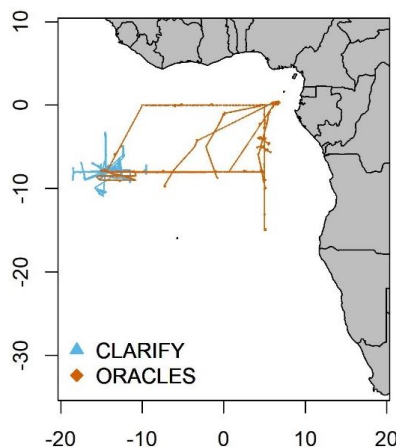
134

135 **Figure 1: Map of AERONET sites used for model evaluation (© Google Earth).**

136 In addition, we evaluate the model's relative aerosol composition against measurements from the Atmospheric
137 Radiation Measurement (ARM) facility on Ascension Island during the LASIC campaign, conducted from January to
138 October 2017. LASIC employed an Aerodyne aerosol chemical speciation monitor (ACSM) to quantify sulfate,
139 nitrate, ammonium, and organic aerosol mass concentrations. Barrett et al. (2022) reported that aerosol mass
140 concentrations of individual components observed by the LASIC ACSM were 2 to 4.5 times lower than those
141 measured by the aerosol mass spectrometer (AMS) aboard the CLARIFY campaign aircraft. Hence, we evaluate the
142 relative rather than absolute aerosol speciation in GEOS-Chem against the LASIC ACSM.

143 **2.3 Aircraft measurements**

144 We evaluate simulated aerosol composition against airborne measurements from two campaigns, NASA ORACLES
145 (Redemann et al., 2021; Ryoo et al., 2021) and UK CLARIFY (Haywood et al., 2021). The ORACLES field campaign
146 used the NASA P-3 aircraft to make measurements based out of São Tomé and Príncipe while CLARIFY used the
147 FAAM BAe-146 aircraft around Ascension Island for data collection. The ORACLES aircraft primarily conducted
148 morning sampling, between 8:00-13:00 UTC, while the CLARIFY aircraft often sampled extended hours, typically
149 from 7:00-18:00 UTC. Both campaigns occurred during the austral winter/spring (August-September), corresponding
150 with peak biomass burning events in southern Africa (Adebisi et al., 2015). Figure 2 shows the flight tracks for these
151 campaigns. The primary instruments and references for each campaign are listed in Table 1.



152

153 **Figure 2: Flight tracks from the two aircraft campaigns used to evaluate the model, CLARIFY (in blue) and ORACLES**
 154 **(in orange), conducted during August-September 2017 over the southeast Atlantic region.**

155 To facilitate comparison between airborne measurements and the GEOS-Chem model, we sampled the model to the
 156 nearest grid box, both temporally and spatially, along the flight tracks. Observations from both campaigns are reported
 157 at 1-minute averaging intervals, while the model operates at a 10-minute temporal resolution (see Sect. 2.1). Aerosol
 158 concentrations from the campaigns are reported as mass concentrations at standard temperature and pressure (STP:
 159 273 K, 1 atm). The modeled concentrations are thus also standardized to STP conditions.

160 **Table 1:** Aircraft campaigns in the southeast Atlantic used for model evaluation during the biomass burning season

Campaign	Date range (Duration)	Instruments*	Aerodynamic Diameter (μm)	Altitude from surface (km)	Primary Reference
CLARIFY	7 th August–4 th September 2017 (99h)	C-ToF-AMS	0.05 to 0.60	0 to 8	Haywood et al., 2021
ORACLES	16 th August–6 th September 2017 (112h)	HR-ToF- AMS	0.07 and 0.70	0 to 7	Redemann et al., 2021

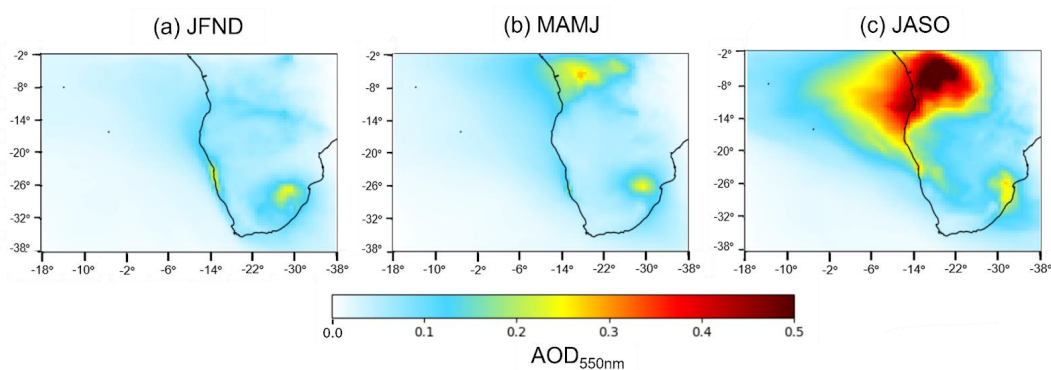
161 *Compact Time-of-Flight (C-ToF), High Resolution Time-of-Flight (HR-ToF), Aerosol Mass Spectrometer (AMS)

162 3.1 Model Evaluation

163 3.1.1 Seasonal variation of AOD



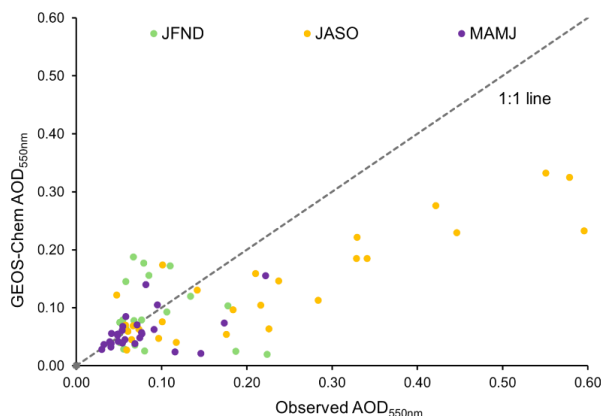
164 The spatial distribution of seasonal mean AOD from GEOS-Chem for the year 2017 is presented in Fig. 3. Three
165 distinct seasonal periods reflect dominant atmospheric and oceanic processes. These include the high DMS emission
166 period in the SEA, during the months of January, February, November, and December (JFND); the peak biomass
167 burning season in southern Africa, spanning from July to October (JASO); and the transitional season, encompassing
168 March, April, May, and June (MAMJ).



169 **Figure 3: Spatial distribution of seasonal mean modeled AOD at 550 nm for 2017. Seasons are as follows: (a) the peak DMS**
170 **emission period (JFND), (b) the transitional period (MAMJ), and (c) the peak biomass burning period (JASO).**
171

172 The simulated DMS emissions, based on Lana climatology (2011), indicates that emissions in the BUS region peak
173 in January, leading to elevated concentrations of sulfate aerosols. This increase, combined with dust emissions from
174 the Namib desert, contributes to an AOD hotspot as depicted in Fig. 3a on the southwestern coast. In the JASO period
175 (Fig. 3c), modeled AOD increases due to biomass burning aerosols, originating from savannah fires in Central and
176 southern Africa and transported westward towards the SEA region by the southern African easterly jet (Adebiyi and
177 Zuidema, 2016). The spatial distribution of mean transitional period AOD (Fig. 3b) features hotspots in Namibia and
178 southern Africa, which coincide with dominant anthropogenic sources and the onset of biomass burning in Central
179 Africa.

180



181

182 **Figure 4: Modeled AOD_{550nm} (Y-axis) with respect to AERONET AOD_{550nm} (X-axis). Each data point represents the**
 183 **monthly mean values for each station color-coded by season (green- DMS period, yellow - biomass burning period, purple-**
 184 **transitional period). The dotted line depicts the 1:1 relationship.**

185 Figure 4 shows the correlation of monthly average AERONET and GEOS-Chem AOD across the nine selected sites
 186 (see Sect. 2.1 and Fig. 1), with the three seasonal periods indicated by color (green for peak DMS emission season-
 187 JFND, yellow for biomass burning season-JASO, and purple for the transition period-MAMJ). Table 2 compiles the
 188 performance of monthly mean GEOS-Chem AOD with respect to AERONET AOD by season. JASO exhibits the
 189 strongest correlation ($R = 0.92$), which is statistically significant ($p < 0.05$). The transitional period (MAMJ) shows a
 190 moderate correlation ($R = 0.51$) with a normalized mean bias (NMB) of -9.5%. A notably low correlation coefficient
 191 ($R = -0.12$) with a positive bias (12.5%) is seen during the summer period (JFND), predominantly due to anomalies
 192 at two sites. This period witnesses a considerable underestimation of AOD at Ascension Island, alongside an
 193 overestimation of dust aerosol at Gobabeb. Excluding these two sites from the analysis, both the correlation coefficient
 194 and NMB improve to 0.61 ($p = 0.55$) and -8% respectively, indicating better model performance at the remaining 7
 195 sites. This underestimate of AOD at Ascension Island (Fig. A1 in the Appendix) during summer (JFND) suggests
 196 potential model limitations in accurately simulating natural aerosol emissions such as sea salt and marine biogenic
 197 emissions. Meanwhile, the AOD discrepancy at Ascension Island in the biomass burning season, may be due to the
 198 underestimate of transatlantic transport of light-absorbing carbon aerosols (Das et al., 2017) and deviations in its
 199 spatial distribution from typical zonal patterns over the Atlantic (Adebisi et al., 2023). Furthermore, Table 2 shows
 200 that the model underestimates AOD during JASO by 26.5% (NMB) across the domain during. This underestimate
 201 may stem from the model's bulk aerosol scheme which inadequately captures the optical properties of aerosols and is
 202 compounded by a low relative humidity bias (Zhai et al., 2021). The bulk scheme also assumes all aerosols are
 203 externally mixed, which contrasts with the variable degree of particle mixing states in the atmosphere (Yu et al., 2012).
 204 Additionally, studies like Hodzic et al. (2020) using NASA ATom aircraft data, indicate that GEOS-Chem
 205 substantially underestimates oxidation levels of organic aerosols in remote areas, which could affect estimates of their
 206 burden and optical properties.



207 Table 2: Statistical parameters of monthly mean modeled AOD with respect to observed AOD at the AERONET sites
 208 by season

Time period	Number of observations	Correlation coefficient (R)	Normalized mean bias (NMB) (%)	Root-mean square error (RMSE)
JFND	20	-0.12 (p = 0.75)	12.5	0.079
MAMJ	26	0.51 (p = 0.15)	-9.5	0.044
JASO	28	0.92 (p = 0.018)	-26.5	0.15

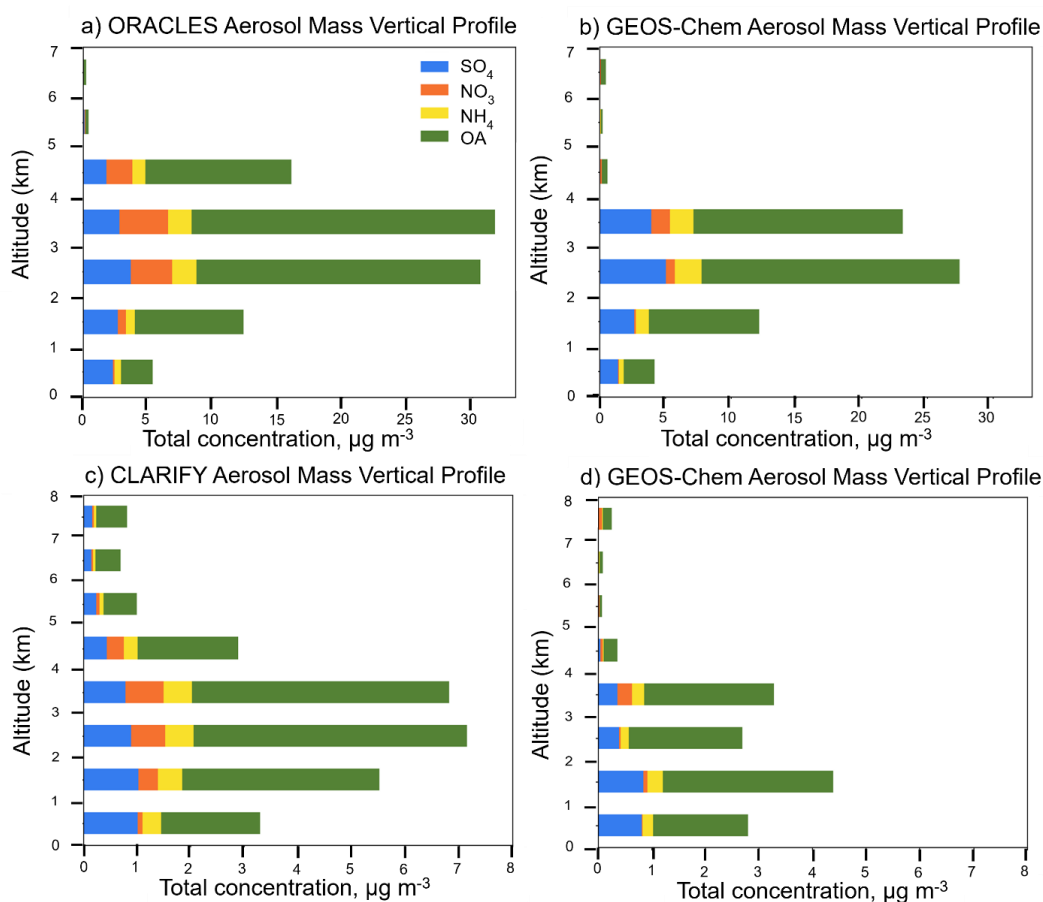
209 We evaluate the relative aerosol speciation simulated at Ascension Island against monthly mean ACSM observations
 210 during the LASIC campaign (see Sect. 2.2) available for January–October 2017 (Fig. A2 in the Appendix). The
 211 seasonality of the relative contributions of organic aerosols and sulfate are consistent between the model and
 212 observations. However, the model underestimates the relative contribution of sulfate during most months, while
 213 generally overestimating the proportion of organics. An increase in the transport of biomass burning organic aerosols
 214 would further worsen the model underestimate of sulfate. The modeled relative contribution of sulfate is closest to
 215 that observed in January and February, when simulated DMS emissions in the region are high (Lana et al., 2011), with
 216 a slight overestimate in the latter.

217 3.1.2 Vertical profiles of aerosol composition

218 Figure 5 depicts the mean vertical profiles of speciated aerosol mass concentrations observed during ORACLES and
 219 CLARIFY aircraft campaigns in August–September 2017 (the biomass burning season), compared to GEOS-Chem
 220 (see Sect. 2.2 and Table 1). The cloud top height in the SEA region generally falls between 0 to 2 km (Redemann et
 221 al., 2021). Findings from Diamond et al. (2018) indicate that aerosols below clouds in this lower atmospheric layer
 222 can also substantially impact cloud microphysics. At these altitudes (0–2 km), GEOS-Chem performs well against
 223 AMS measurements of total aerosol mass, which includes sulfate, nitrate, ammonium and organics from these
 224 campaigns, with an NMB between -3.5% (CLARIFY) to -7.5% (ORACLES). At mid-altitudes (2–4 km), the model
 225 achieves moderate agreement, with NMB values spanning -19% (ORACLES) to -57% (CLARIFY). However, the
 226 model demonstrates a pronounced bias at higher altitudes (4–7 km), where NMB values drop to -92% (ORACLES)
 227 to -93.5% (CLARIFY), underscoring challenges in accurately modeling aerosol concentrations at these elevations. Pai
 228 et al. (2020) suggests that the model underestimation of organic aerosol loading at mid-tropospheric heights is linked
 229 to the surface injection treatment of fire emissions in GFED4.1s. Recent studies by Wizenberg et al. (2023) and Marvin
 230 et al. (2024) concur that fire injection scheme is a critical source of model uncertainty, emphasizing the potential



231 importance of accurate fire injection modeling in the free troposphere. Nonetheless, our study focuses on aerosol
 232 composition within cloud-relevant altitudes to improve our understanding of aerosol-cloud interactions and their
 233 climate implications. The observed vertical distribution of aerosol mass concentrations (left panels of Fig. 5), indicates
 234 that 18% and 36% of the aerosol mass for the ORACLES and CLARIFY campaigns, respectively, is located below 2
 235 km, within columns extending up to flight altitudes of 7 km and 8 km. However, the model simulates elevated aerosol
 236 mass at these lower altitudes, 24% and 50% of the column for ORACLES and CLARIFY, respectively.



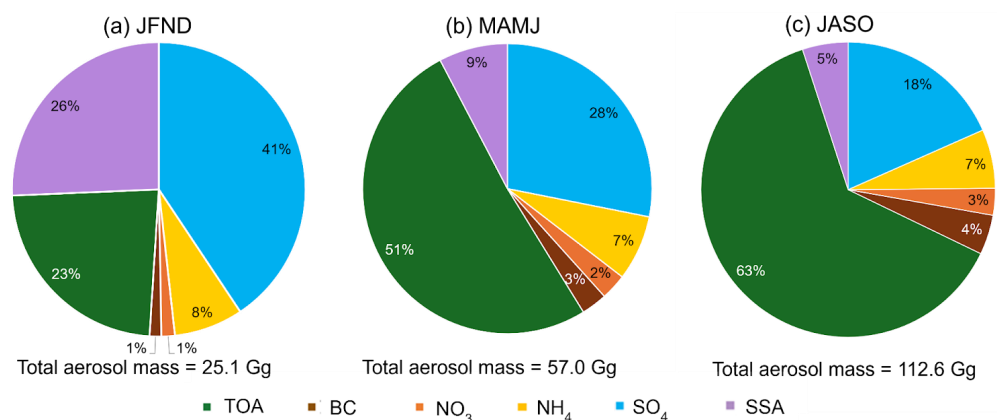
237
 238 **Figure 5: Average vertical profiles of simulated and observed aerosol mass during August–September 2017 (peak biomass**
 239 **burning season) from aircraft campaigns. The left column presents the vertical distribution of aerosols observed during the**
 240 **ORACLES flight campaign (panel a) and the CLARIFY flight campaign (panel c) at STP (see Sect. 2.3). The right column**
 241 **displays the GEOS-Chem model simulations along the respective flight tracks of each campaign (panels b and d). All data**
 242 **are averaged over 1 km vertical bins.**

243 At altitudes where clouds persist in the domain (0 to 2 km), sulfate and organic aerosols are the dominant aerosol
 244 types. Here, the model effectively captures the mass concentration of organic aerosols, with an NMB ranging from -



245 0.40% for ORACLES to -14% for CLARIFY. However, it underestimates sulfate aerosol concentrations by 19% at
 246 cloud altitudes for both campaigns. For other aerosol types and altitudes, the model consistently underestimates
 247 concentrations, except for sulfate and ammonium aerosols between 2 to 4 km during the ORACLES campaign, which
 248 the model overestimates by 40% and 4.6%, respectively. The model captures the total aerosol mass from 0 through 7
 249 km for sulfate and ammonium aerosols during the ORACLES campaign, with only minimal underestimations of 1.5%
 250 and 0.7%, respectively. This indicates a potential discrepancy in the vertical distribution of these aerosols rather than
 251 in total mass.

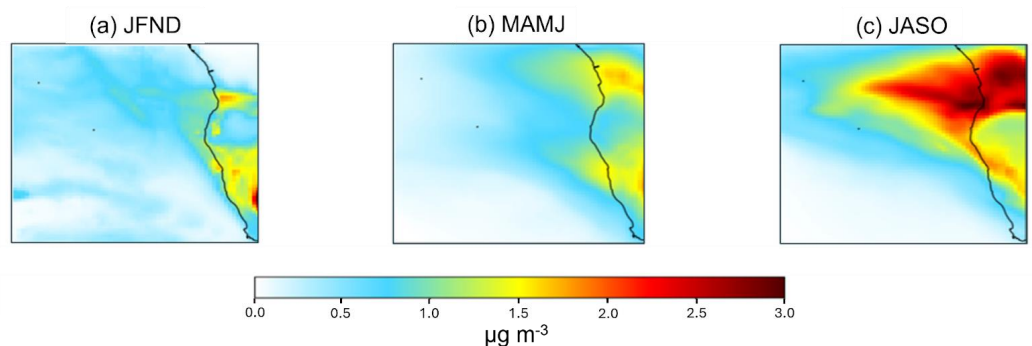
252 3.2 Seasonal variation in aerosol composition and sources at cloud altitudes



253

254 **Figure 6: Simulated mean fractional aerosol composition at cloud heights (0–2 km) over the ocean in the stratocumulus**
 255 **sub-domain (0–35° S, 20° E–20° W) by season: (a) JFND, (b) MAMJ, and (c) JASO. Here SO₄, NH₄, NIT, BC, TOA, SSA**
 256 **represents sulfate, ammonium, nitrate, black carbon, total organic aerosol and accumulation-mode sea salt aerosols,**
 257 **respectively.**

258 Figure 6 presents the simulated seasonal mean aerosol fractional composition within cloud-relevant altitudes (0–2 km),
 259 averaged over the ocean only across the subdomain (0–35° S, 20° E – 20° W) (see the map shown in Fig. 7). This area
 260 is strategically selected to coincide with the persistent Sc cloud deck and enhance our analysis of aerosol-cloud
 261 interactions. Organic aerosols, an indicator of biomass burning, predominate during both the biomass burning (JASO)
 262 and transitional (MAMJ) periods. In contrast, sulfate aerosols dominate during austral summer, likely influenced by
 263 the high primary production from coastal upwelling that leads to DMS emissions. We investigate the model
 264 representation of sulfate and these processes further in subsequent sections. An increase in the accumulation-mode
 265 sea-salt aerosols (radius 0.01–0.5 μm) contribution (total mass of 6.7 Gg) is observed in summer (Fig. 6a) as well,
 266 compared to other seasons (5.2 Gg during MAMJ and 5.8 Gg during JASO), owing to the peak wind speeds in the
 267 southern Benguela region in this season (Hutchings et al., 2009). Black carbon, ammonium, and nitrate aerosols make
 268 minor contributions to simulated aerosol mass at cloud height throughout the year.



269

270 **Figure 7: Spatial distribution of simulated mean sulfate aerosol concentrations averaged over cloud altitudes (0–2 km) in**
 271 **the sub-domain (0–35° S, 20° E–20° W) by season in 2017: (a) peak DMS emission season (JFND), (b) transitional phase**
 272 **(MAMJ), and (c) biomass burning season (JASO).**

273

3.2.1 Drivers of sulfate aerosol and importance of marine precursor emissions

274

Sulfate aerosols are the most or 2nd most important aerosol component in cloud heights over the SEA (Fig. 6). We
 275 examine the sources of sulfur emissions within the model in Figure A3. Within the broader domain (0–40° S, 40° E–
 276 20° W), anthropogenic activities are the largest source of sulfur emissions throughout the year (Fig. A3), followed by
 277 DMS emissions from the ocean. DMS emissions become more pronounced during the austral summer, peaking in
 278 January. Additionally, biomass burning contributes to SO₂ emissions seasonally, becoming the 3rd most important
 279 source of total sulfur emissions during July - September (Fig. A3).

280

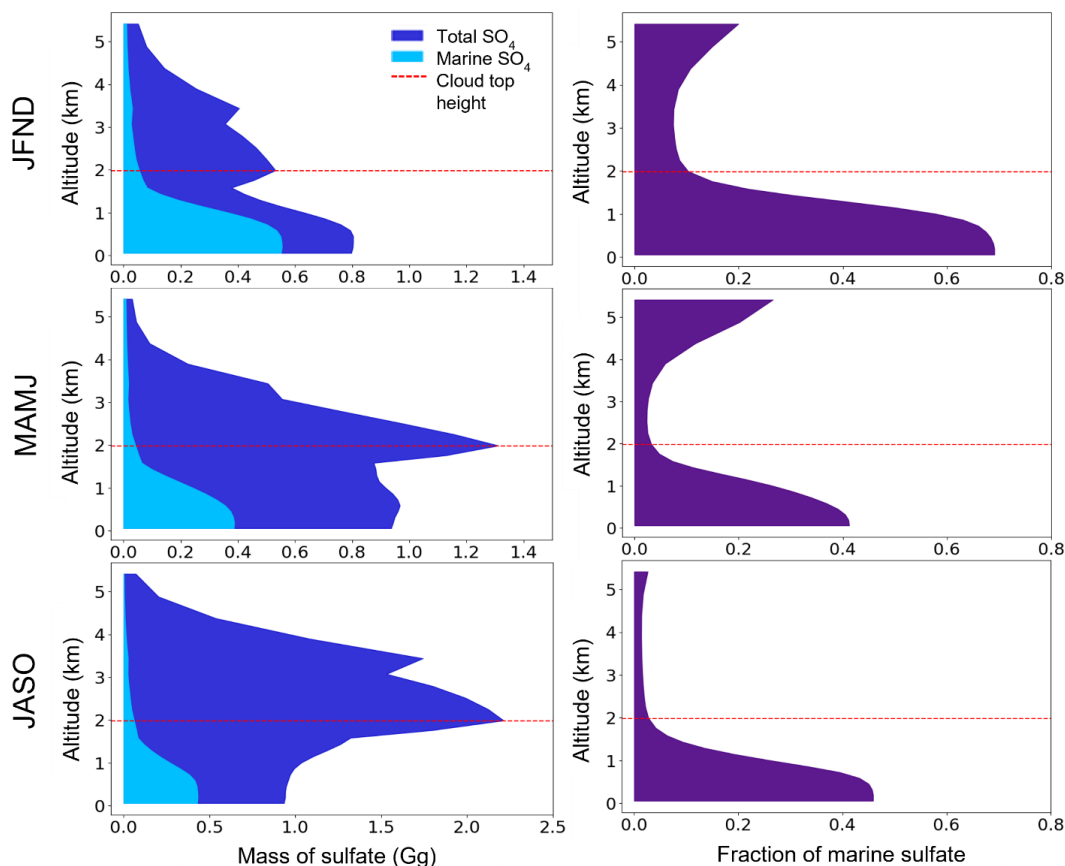
To improve understanding of the processes driving sulfate aerosol concentrations in the region, we examine its
 281 simulated spatial distribution averaged by season over the cloud height (0–2 km) in Fig. 7. Elevated concentrations of
 282 DMS, resulting from higher rates of primary production (Lana et al., 2011; Galí et al., 2018), lead to an increase in
 283 sulfate concentrations along the coastline of the Benguela region and the inner shelf of Namibia during JFND (Fig.
 284 7a), aligning with the AOD hotspot observed in Fig. 3a. This is consistent with the simulated dominance of sulfate
 285 aerosols at cloud-relevant altitudes during JFND (Fig. 6a). During the biomass burning months (JASO), while their
 286 relative contribution decreases (Fig. 6c), sulfate aerosols display a pronounced increase in absolute concentration (Fig.
 287 7c) as a consequence of savanna fire emissions from southwestern Africa (van der Werf et al., 2010; Das et al., 2017).
 288 As outlined in the AOD evaluation (Sect. 3.1.1), the model underestimates the transport of emissions to remote sites
 289 (Fig A1), resulting in a steep gradient in sulfate concentrations from the eastern landmass towards the western open
 290 ocean.

291

To quantitatively estimate the contribution of marine precursor emissions to sulfate aerosols, we compare the sulfate
 292 mass between the standard and marine emissions only sensitivity simulations (Sect. 2.1). Figure 8 shows seasonally
 293 averaged vertical profiles over the ocean region of the Sc sub-domain (0°–35° S, 20° E–20° W). The figure presents
 294 the marine-only sulfate mass and the total sulfate mass from the standard simulation (left panels), and the ratio of
 295 marine sulfate to total sulfate (right panels). Vertical profiles were computed by summing the sulfate mass within each



296 grid box, scaled by the grid box ocean fraction, across latitude and longitude within each vertical layer of the model,
 297 and then averaged temporally across each season.



298

299 **Figure 8: Simulated vertical profiles of sulfate aerosol mass over oceanic regions within the sub-domain (0°–35° S, 20° E–**
 300 **20° W) by season. The left panel shows the mass of total and marine sulfate aerosols, and the right panel indicates the sulfate**
 301 **fraction from marine sources. The top row corresponds to the peak dimethyl sulfide (DMS) emission period (JFND); the**
 302 **middle row to the transitional period (MAMJ); and the bottom row to the peak biomass burning period (JASO) (note: the**
 303 **bottom left panel displays a higher x-axis scale). The upper red dashed line denotes the typical maximum cloud top height**
 304 **(Redemann et al., 2021).**

305 Our analysis highlights the substantial influence of marine sulfur sources on sulfate during JFND, as evidenced in the
 306 top left panel of Fig. 8. During this period the proportion of marine sulfate reaches up to 69.1% within-cloud (from
 307 surface to 2 km). The contribution of marine sulfate within the cloud in the subsequent periods is reduced (ranging
 308 between 2.7–45.9%; Fig. 8). We find that marine-sourced sulfate mass remains fairly consistent throughout the year
 309 (Fig. 8, left panels), with variations in the marine sulfate fraction (Fig. 8, right panels) mainly due to changes in land-
 310 based sulfate sources. Total sulfate mass during seasons influenced by biomass burning (MAMJ and JASO) peaks at



311 2 km, with greater mass above 2 km during peak biomass burning (JASO) in contrast to JFND where mass peaks
312 within clouds (0–2 km).

313 Table A3 summarizes the monthly mean percent contribution of marine sulfate averaged across cloud altitudes (0–
314 km). The annual average total sulfate mass and marine sulfate mass is 16.2 Gg and 3.5 Gg, respectively. The within-
315 cloud marine sulfate contribution peaks in January (57.7%) and is smallest in September (10.3%). Thus, our analysis
316 suggests that DMS emissions influence sulfate aerosol formation and their interactions with clouds in the region
317 throughout most of the year, excepting only the peak biomass burning season. This emphasizes that constraining
318 marine sulfur sources and chemistry both in chemical transport and climate models may improve representation of
319 aerosol-climate dynamics in the SEA region. Limited available observations suggest the model is biased low in AOD
320 throughout most of the year (Sect. 3.1.1), and underestimates sulfate aerosol concentrations in August and September
321 at cloud altitudes (Sect. 3.1.2, Fig. 5). We explore related uncertainties and their implications in the following
322 sections.

323 **3.3 Uncertainties**

324 **3.3.1 Assessing variations in DMS emission rates and oxidation mechanism on sulfate aerosol formation**

325 The Benguela region has substantial uncertainties in DMS concentrations in surface seawater and the corresponding
326 emission fluxes owing to the limited availability of biogenic sulfur measurements. To investigate the sensitivity of
327 DMS emission fluxes to changes in surface seawater DMS concentrations, we conducted two simulations with DMS
328 concentrations from Lana et al. (2011) and Galí et al. (2018) (see Sect. 2.1). The standard results presented thus far
329 were conducted using the Lana dataset.

330 In the southern Benguela, south of approximately 27° S, marked upwelling during the austral summer (Shannon and
331 Nelson, 1996; Hutchings et al., 2009) promotes phytoplankton growth and elevates DMS emissions. Although the
332 Lana dataset indicates that DMS emission fluxes over the Sc sub-domain peak in January (Fig. A4 of the Appendix),
333 coinciding with this phenomenon, it lacks clear seasonality for the remaining months. In contrast, satellite-based DMS
334 estimates from Galí show pronounced emissions throughout the austral summer (JFND), as shown in Fig. A4. Both
335 datasets concur in magnitude for January and February, a period with better data coverage in the Lana et al. (2011)
336 climatological data set over the domain. However, the Lana dataset DMS emissions are up to 38% less during
337 December, while 51% higher in July relative to the Galí dataset (Ghahreman et al., 2019). This suggests the marine
338 contribution to sulfate in our standard simulation using the Lana dataset may be underestimated from October through
339 December (encompassing two months of the peak DMS season) and overestimated from March through August (Fig.
340 A4).

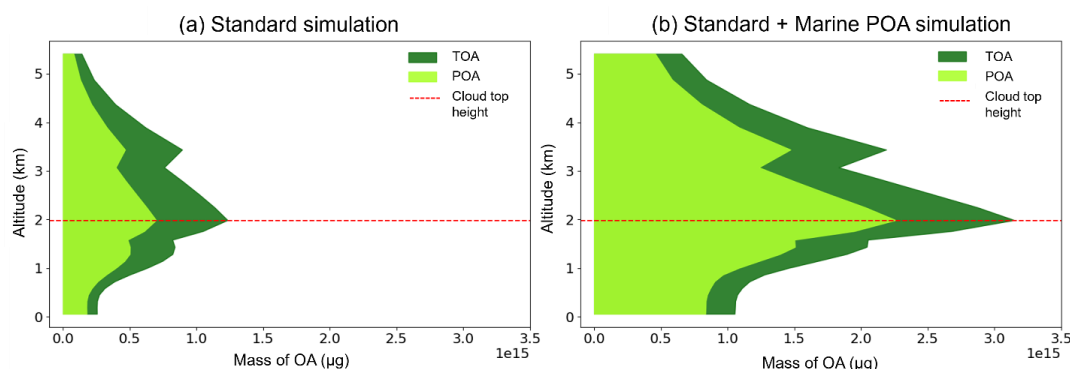
341 The ongoing discovery of complexities within DMS oxidation mechanisms, along with the incomplete incorporation
342 of these mechanisms into atmospheric chemistry models, further contributes to uncertainties in predicting the impact
343 of DMS emissions on aerosols and climate (Faloona, 2009; Quinn and Bates, 2011; Carslaw et al., 2013). Chen et al.
344 (2018) highlighted the impacts of changes to DMS chemistry in the GEOS-Chem model, integrating a series of



345 multiphase sulfur oxidation mechanisms and two DMS intermediates, which led to a decrease in the global DMS
 346 burden, thereby decreasing SO₂ and sulfate levels. On the other hand, Novak et al. (2021) found that the cloud uptake
 347 of hydroperoxymethyl thioformate (HPMTF), a newly identified oxidation product of DMS (Wu et al., 2015; Veres
 348 et al., 2020), lowers near-surface SO₂ concentration while elevating sulfate concentration in the model. Most recently,
 349 Tashmim et al. (2024) implemented an advanced DMS oxidation mechanism in GEOS-Chem that incorporates the
 350 latest developments in DMS chemistry, including those previously mentioned, which led to a lower SO₂ mixing ratio
 351 (~70%) and a higher SO₄ mixing ratio (~35%) over the SEA during austral summer. Thus, an improved representation
 352 of DMS emissions and oxidation chemistry in the model could enhance the sulfate aerosol estimations during the peak
 353 DMS season. This refinement may address model underestimates of aerosol concentrations during this period (Sect.
 354 3.1.1).

355 3.3.2 Exploring the impact of marine organic aerosol emissions on organic aerosol concentrations

356 Beyond marine sulfate and sea-salt aerosols, organic matter also makes a significant contribution to marine aerosol
 357 mass (Middlebrook et al., 1998; Oppo et al., 1999; Russell et al., 2010). Notably, substantial concentrations of organic
 358 carbon aerosols have been observed in marine regions, particularly during periods of intense biological activity
 359 (O'Dowd et al., 2004). These aerosols can also increase CCN, affecting cloud properties and radiative balance (Arnold
 360 et al., 2009; Gantt and Meskhidze, 2013). However, the standard GEOS-Chem model does not account for these
 361 organic aerosol emissions. We analyzed the impact of marine POA on cloud-altitude aerosols over the SEA by
 362 incorporating POA emissions based on satellite-derived chlorophyll-a concentrations (Gantt et al., 2015; See Sect.
 363 2.1) in the model.



364

365 **Figure 9: Vertical distribution of organic aerosol mass during November 2017, the month of maximum discrepancy between**
 366 **the standard and MPOA simulations, over the Sc sub-domain (0–35° S, 20° E–20° W). Left: mass profile for total organic**
 367 **aerosols (TOA) and primary organic aerosols (POA) under standard simulation conditions (Std); right: when marine**
 368 **primary organic aerosol (MPOA) emissions are included (Std + MPOA). The red dashed line indicates the typical maximum**
 369 **cloud top height.**



370 We find that the inclusion of MPOA emissions consistently resulted in higher organic aerosol mass, with the greatest
371 increase in November. Figure 9 shows the vertical distribution of total organic aerosols (TOA) mass and POA mass
372 (including MPOA and other POA sources) with and without MPOA emissions during this month. Similar to our earlier
373 vertical profile analysis (refer to Sect. 3.2.2), we find that the maximum organic aerosol mass occurred at the highest
374 cloud top height (2 km). The Standard + MPOA simulated peak total organic aerosol mass was approximately three
375 times higher than that in the Standard simulation, highlighting the potential contribution of marine sources to total
376 organic aerosol mass concentrations. However, during the biomass burning season, the sensitivity simulation showed
377 only a minimal increase, indicating that it does not adequately address the model's underestimation (refer to Fig. 5).
378 Gantt et al. (2015) demonstrated that including MPOA emissions in GEOS-Chem reduced the normalized mean bias
379 (NMB) of surface organic aerosol concentrations at coastal sites by 67%. Additionally, Pai et al. (2020) noted that
380 without a marine POA source, the model fails to accurately reproduce lower-tropospheric concentrations over oceans,
381 although the marine POA scheme might be biased high. Despite the limitations of a chlorophyll-based
382 parameterization like the one used here in providing mechanistic understanding of the seasonal and geographical
383 variability of organic matter emissions from sea spray (Burrows et al., 2022), our findings suggest that MPOA may
384 play a role in aerosol-cloud interactions outside of the biomass burning season, in addition to marine-derived sulfate
385 from DMS (Sect. 3.2).

386 **3.3.3 Impacts of uncertainties in biomass burning emissions of SO₂**

387 To assess the impact of uncertainty in biomass burning emissions of SO₂ on the relative contribution of marine vs.
388 land sources to aerosol, we performed a sensitivity analysis using two alternative inventories, QFED and GFAS (see
389 Sect. 2.1 and Table-A2). The standard simulations, as detailed in Sect. 2.3, use the default biomass burning inventory
390 in GEOS-Chem, GFED. The GFAS inventory SO₂ and CO emissions over the domain are constant in time, aligning
391 with QFED during the non-biomass burning months (Fig. A5). We find that CO emissions from GFED and QFED
392 align closely; however, there is a notable difference in SO₂ emissions between the two inventories (Fig. A5). These
393 discrepancies likely originate from variations in SO₂ emission factors employed by each inventory. In July, which
394 exhibits the largest difference between the two inventories, peak SO₂ emissions in QFED are almost five-fold higher
395 than those in GFED. This discrepancy leads to a 25% increase in sulfate aerosol concentrations at cloud altitudes
396 relative to the standard results using GFED (not shown). Consequently, the contribution of marine sulfate to total
397 sulfate (see Sect. 3.2.1) may further decrease during the peak biomass burning season if QFED is used, highlighting
398 the sensitivity of aerosol source attributions to the selected biomass burning inventory.

399 **4 Implications**

400 In this study, monthly marine sulfate constitutes between 10.3% and 57.7% of total sulfate within the cloud height,
401 peaking during the high DMS emission period. However, the default Lana et al. (2011) climatology largely
402 underestimates DMS emissions during the austral summer (November and December) by up to 38%, compared to the
403 satellite-derived estimates from Galí et al. (2018). Moreover, improvement of DMS chemistry in the model by
404 incorporating new oxidation mechanisms and intermediate products could shift the balance towards increased sulfate



405 aerosol production (with Tashmim et al., 2024 suggesting an increase of up to 35% over the SEA). Marine primary
406 organic aerosol emissions may also contribute substantially to the organic aerosol mass during the peak primary
407 production period (JNFD), highlighting the importance of marine contributions to overall aerosol concentrations.
408 Meanwhile, discrepancies in SO₂ emissions from biomass burning can increase sulfate aerosol from biomass burning
409 by up to 25%. These changes would improve the model underestimate of AOD relative to AERONET observations;
410 however, observations of aerosol composition outside of August-September are very limited and this is a large gap.
411 Our results suggest marine-sourced sulfate and organics significantly influence aerosol loading and composition in
412 the SEA, particularly during the non-biomass burning period. Accurately characterizing the seasonal dynamics of
413 aerosols within cloud heights is imperative for quantifying aerosol-cloud interactions and understanding the dynamics
414 of marine aerosols in the SEA region, where uncertainties in aerosol radiative forcing are most pronounced. This
415 understanding is essential for improving the reliability of climate models in areas critical to both regional and global
416 climate dynamics.

417 **5 Conclusion**

418 Aerosols over the southeast Atlantic strongly influence global climate dynamics due to the presence of persistent
419 stratocumulus clouds and large uncertainties in aerosol-cloud interactions. However, precisely representing these
420 interactions in global climate models remains challenging, in part due to sparse available observations, especially
421 outside of the biomass burning season. In this study, we employed the GEOS-Chem chemical transport model to
422 assess the aerosol composition at cloud-relevant altitudes (0–2 km) and identify the sensitivities to marine emissions
423 and chemistry in the southeast Atlantic. This analysis aims to enhance our understanding of the role of marine aerosols
424 and the associated uncertainties affecting aerosol-cloud interactions within this climate-sensitive region.

425 We performed nested grid simulations with a 0.5° x 0.625° horizontal resolution and evaluated the model against
426 ground-based and aircraft campaign observations throughout 2017. We analyzed results for three seasonal periods
427 with distinct dominant processes including (a) the high DMS emission season (JFND), (b) the peak biomass burning
428 season (JASO), and (c) the transitional season (MAMJ). Our analysis showed that simulated monthly average aerosol
429 optical depth (AOD) exhibits the strongest correlation ($R = 0.92$) with the AERONET AOD observations during the
430 JASO season. However, the model generally underestimates AOD throughout the year, except in the JFND period.
431 These underestimations are primarily due to limitations in representing natural aerosol emissions, transatlantic aerosol
432 transport, particle mixing states, and the oxidation levels of organic aerosols. Moreover, a comparison of aerosol
433 speciation measured at Ascension Island during the LASIC campaign indicates that the model consistently
434 underestimates sulfate aerosols. We further evaluated the simulated vertical profile of aerosol mass concentrations
435 and composition against measurements from the ORACLES and CLARIFY campaigns. These comparisons showed
436 that sulfate aerosols were underestimated by 19% at cloud-relevant altitudes of 0–2 km by both campaigns. However,
437 discrepancies increase with altitude, reflecting challenges in accurately modeling high-altitude aerosol concentrations.

438 Analysis of seasonal mean aerosol composition at cloud height showed that organic aerosols predominate during
439 JASO (63%) and MAMJ (51%), while sulfate aerosols are most prevalent (41%) during the austral summer (JFND).



440 Given the prominence of sulfate as a marine sourced aerosol in remote oceanic environments, we investigated the
441 processes influencing the sulfate aerosol concentrations in our domain. Throughout the year, anthropogenic sources
442 and oceanic DMS emissions are the primary atmospheric sulfur contributors. Spatial mapping across the sub-domain
443 (0–35° S, 20° E–20° W) showed high sulfate concentrations (up to $3\mu\text{g m}^{-3}$) at cloud height during the peak biomass
444 burning season (JASO), primarily from savannah fires in southern Africa. Despite this, sulfate aerosols only account
445 for 18% of the total aerosol mass in JASO.

446 Sulfate, primarily from marine sources, is the dominant aerosol at cloud-relevant altitudes during JFND in the model
447 (up to 69% marine contribution); however, significant uncertainties regarding the treatment of DMS persist that may
448 affect this finding. To assess the impact of these uncertainties on sulfate aerosols, we compared DMS emission fluxes
449 from Lana et al. (2011) climatological data and Galí et al. (2018) satellite-based estimates of surface seawater DMS
450 concentrations. The limited spatial and temporal coverage of the Lana dataset across our domain resulted in a 51%
451 overestimate in emissions in July and a 38% underestimate in December relative to Galí. Moreover, improvement of
452 DMS chemistry in the model by incorporating new oxidation mechanisms and intermediate products could shift the
453 balance towards increased sulfate aerosol production (with Tashmim et al., 2024 suggesting an increase of up to 35%
454 over the SEA). Additionally, emissions of marine primary organic aerosols during the peak primary production period
455 (JNFD) may substantially contribute to the mass of organic aerosols which can also act as CCN. This emphasizes the
456 critical role of marine sources in influencing aerosol concentrations, even in oceanic regions impacted by large
457 seasonal biomass burning. Variations in SO_2 emissions from biomass burning could potentially increase sulfate
458 aerosol concentrations at cloud altitudes by up to 25%. Addressing these discrepancies is essential for improving the
459 model's underestimation of AOD and aerosol concentrations compared to observations.

460 This study highlights the importance of constraining marine emissions and their chemical transformations by
461 incorporating satellite-retrieved datasets and extending field campaign efforts during non-biomass burning periods.
462 Such initiatives are essential to accurately characterize seasonal aerosol dynamics at cloud heights and to improve our
463 understanding of aerosol-cloud interactions in regions with persistent low-altitude clouds. These advancements could
464 substantially minimize uncertainties in model estimates of radiative forcing and enhance the reliability of climate
465 model projections in the southeast Atlantic region.

466

467

468

469

470

471



472 **Appendix A**

473 **Table A1:** Configuration of sensitivity analysis simulations

Simulations	Resolution
Marine sulfur emissions only	0.5° x 0.625°
DMS emissions	4° x 5°
Biomass burning inventories	4° x 5°
Marine primary organics	0.5° x 0.625°

474

475

476 **Table A2:** AERONET site information and the average value (± 1 standard deviation) for AOD₅₅₀ per site are shown.

Site	Latitude (°)	Longitude (°)	Months of data availability for 2017	Daily Average AOD _{550nm} ± 1 SD
Ascension Island	-7.976	-14.415	7	0.18 \pm 0.04
Gobabeb	-23.562	15.041	12	0.10 \pm 0.04
HESS	-23.273	16.503	10	0.08 \pm 0.04
Henties_Bay	-22.095	14.26	3	0.25 \pm 0.02
Lubango	-14.958	13.445	9	0.16 \pm 0.05
Namibe	-15.159	12.178	8	0.33 \pm 0.12
Simonstown_IMT	-34.193	18.446	7	0.05 \pm 0.03
Upington	-28.379	21.156	8	0.08 \pm 0.06
Windport	-19.366	15.483	10	0.15 \pm 0.08

477

478

479



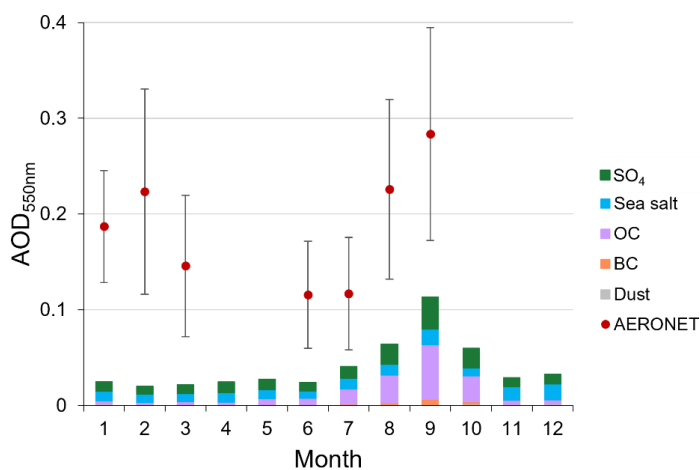
480 **Table A3:** Seasonal variation of percentage of monthly mean percent contribution of marine sulfate within cloud
481 height

Month	Percentage of marine sulfate
January	57.7
February	54.8
March	25.3
April	26.6
May	15.3
June	15.0
July	14.8
August	14.7
September	10.3
October	22.4
November	39.1
December	44.3

482

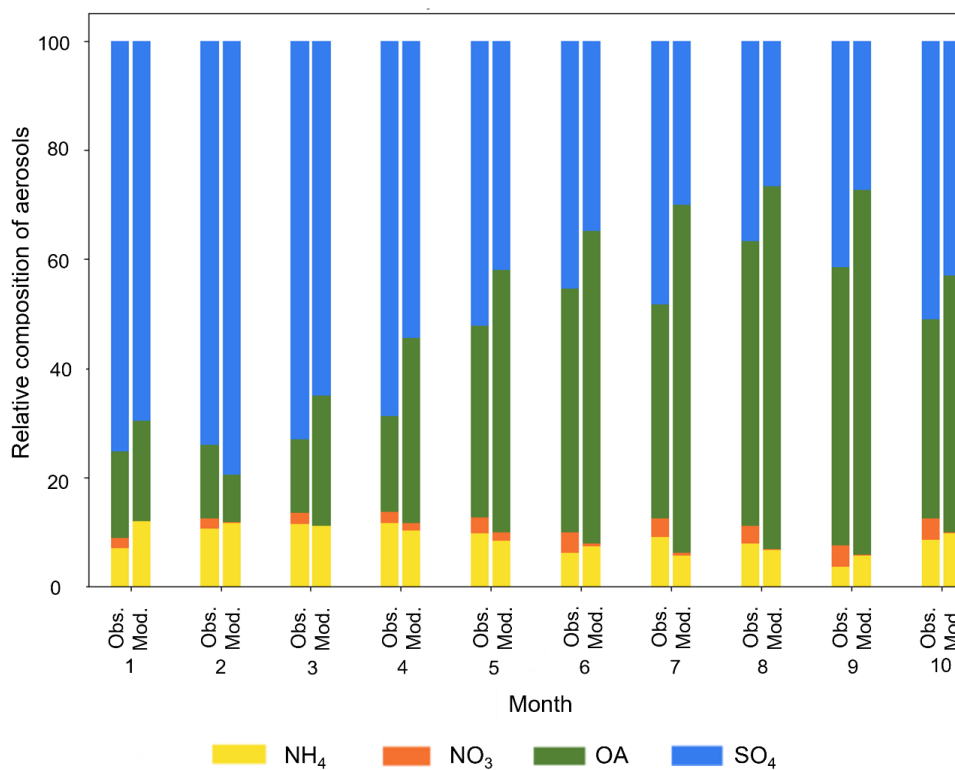
483

484



485

486 **Figure A1:** Comparative analysis of aerosol optical depth at 550 nm (AOD_{550nm}) for Ascension Island in 2017. The
487 red dots present the measured mean monthly AOD values, with vertical error bars illustrating the range of AOD_{550nm}
488 measurements captured by the AERONET ground station. The stacked bars represent the GEOS-Chem model's
489 simulated AOD values, with each layer corresponding to the major aerosol components, such as sulfate (SO₄), sea
490 salt, organic carbon (OC), black carbon (BC), and dust, providing insight into the model's aerosol composition
491 representation.



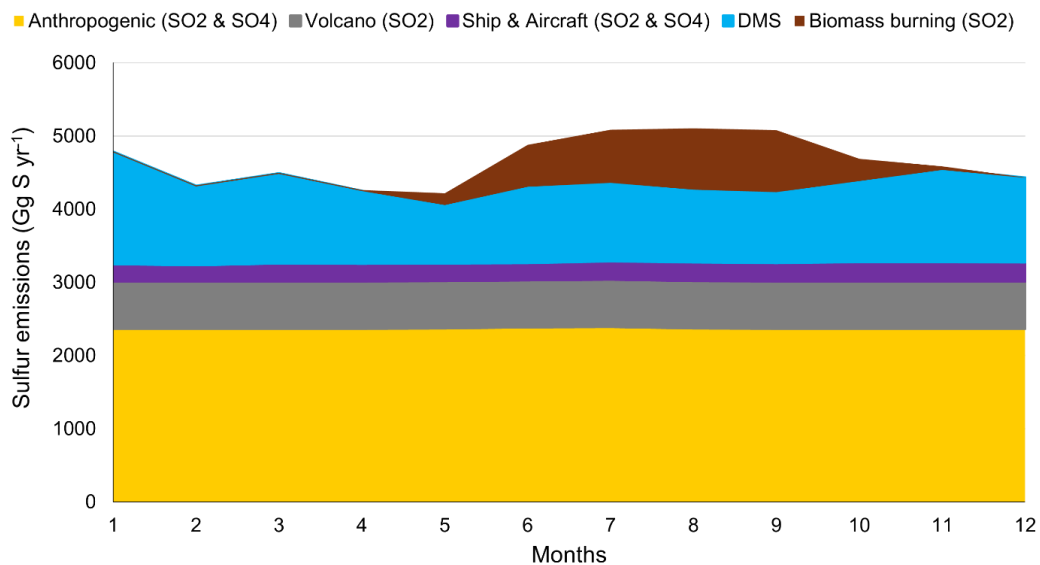
492

493 **Figure A2:** Comparative analysis of the relative aerosol composition at Ascension Island in 2017. The stacked bars
494 on the left depict observations of chemical composition taken during the LASIC campaign at the ARM facility on
495 Ascension Island, utilizing an aerosol chemical speciation monitor (ACSM) at 341 meters. The bars on the right
496 illustrate the GEOS-Chem simulated aerosol composition at the same altitude. Each segment of the stack represents
497 different aerosol components: ammonium (NH₄), nitrates (NIT), organic aerosols (OA), and sulfate (SO₄).

498

499

500



501

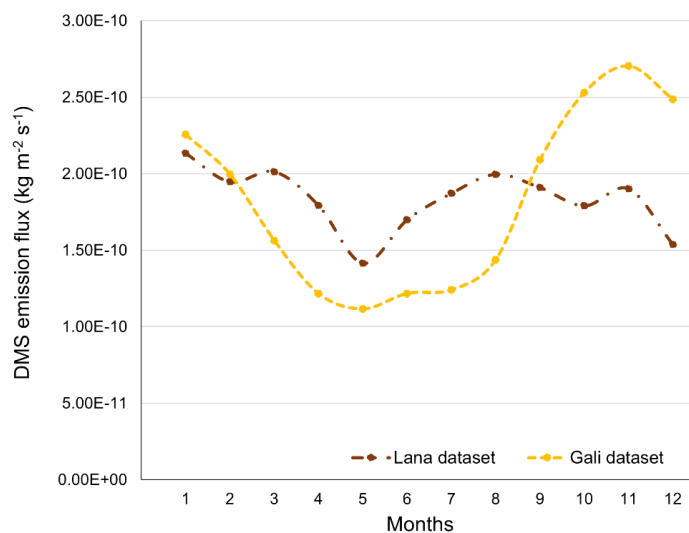
502 **Figure A3:** Stacked area chart of monthly total sulfur emissions by source for 2017 across the study domain (0–40°
503 S, 40° E–20° W) in gigagrams of sulfur per year (Gg S yr⁻¹). Sources are indicated by color and encompass
504 anthropogenic activities, volcanic activity, ship and aircraft emissions, biomass burning and natural emissions of
505 dimethyl sulfide (DMS).

506

507

508

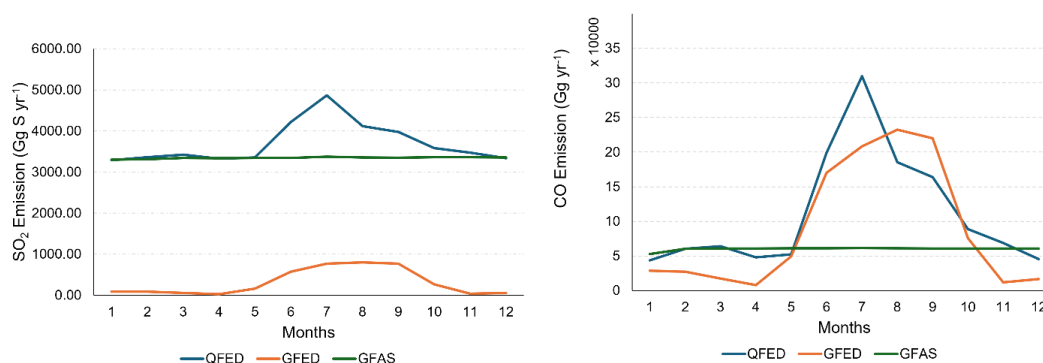
509



510

511 **Figure A4:** Monthly DMS emissions over the stratocumulus sub-domain (0–35° S, 20° E–20° W) using two distinct
 512 datasets for surface seawater DMS concentrations. The brown dashed line presents emissions calculated using Lana
 513 et al. (2011) climatology, which compiles data across 1972–2009 from multiple sources. In contrast, the yellow dashed
 514 line depicts emissions based on satellite-derived estimates of surface seawater DMS concentrations (Galí et al., 2018).

515



516

517 **Figure A5:** Comparison of biomass burning emissions across various inventories, namely GFED, QFED, and GFAS
 518 across the domain (0–40° S, 40° E–20° W). The panels depict the interannual variability of biomass burning emissions,
 519 with the left panel illustrating sulfur dioxide (SO₂) emissions, and the right panel displaying carbon monoxide (CO)
 520 emissions. Both GFED and QFED indicate similar emission trends; however, GFED exhibits lower SO₂ emission
 521 magnitudes compared to QFED. GFAS presents emission magnitudes similar to QFED during non-biomass burning
 522 period.



Author contributions

MH, HMH, and RMG designed the research. MH conducted the model simulations, analysis, and visualization, with expert advice from HMH. MH drafted the manuscript, which was then revised by all co-authors.

Competing interests

At least one of the (co-)authors is a member of the editorial board of Atmospheric Chemistry and Physics.

Acknowledgements

Mashiat Hossain and Hannah M. Horowitz gratefully acknowledge Michael Diamond for discussions on cloud-relevant altitudes over the southeast Atlantic region.

References

- Adebiyi, A. A., and Zuidema, P.: The role of the southern African easterly jet in modifying the southeast Atlantic aerosol and cloud environments, *Q. J. Roy.*, 142, <https://doi.org/10.1002/qj.2765>, 2016.
- Adebiyi, A. A., Zuidema, P., and Abel, S. J.: The convolution of dynamics and moisture with the presence of shortwave absorbing aerosols over the southeast Atlantic, *JCLI*, 28, <https://doi.org/10.1175/JCLI-D-14-00352.1>, 2015.
- Adebiyi, A. A., Akinsanola, A. A., and Ajoku, O. F.: The Misrepresentation of the Southern African Easterly Jet in Models and Its Implications for Aerosol, Clouds, and Precipitation Distributions, *JCLI*, 36, <https://doi.org/10.1175/JCLI-D-23-0083.1>, 2023.
- Alexander, B., Park, R. J., Jacob, D. J., and Gong, S.: Transition metal-catalyzed oxidation of atmospheric sulfur: Global implications for the sulfur budget. *J. Geophys. Res.*, 114, <https://doi.org/10.1029/2008JD010486>, 2009.
- Andreae, M. O.: Ocean-atmosphere interactions in the global biogeochemical sulfur cycle, *Mar. Chem.*, 30, [https://doi.org/10.1016/0304-4203\(90\)90059-L](https://doi.org/10.1016/0304-4203(90)90059-L), 1990.
- Andreae, M. O., Elbert, W., and De Mora, S. J.: Biogenic sulfur emissions and aerosols over the tropical South Atlantic. 3. Atmospheric dimethylsulfide, aerosols and cloud condensation nuclei, *J. Geophys. Res.*, 100, <https://doi.org/10.1029/94jd02828>, 1995.
- Arnold, S. R., Spracklen, D. V., Williams, J., Yassaa, N., Sciare, J., Bonsang, B., Gros, V., Peeken, I., Lewis, A. C., Alvaïn, S., and Alvaïn, M.: Evaluation of the global oceanic isoprene source and its impacts on marine organic carbon aerosol, *Atmos. Chem. Phys.*, 9, <https://doi.org/10.5194/acp-9-1253-2009>, 2009.
- Barnes, I., Hjorth, J., and Mihalopoulos, N.: Dimethyl sulfide and dimethyl sulfoxide and their oxidation in the atmosphere, *Chem. Rev.*, 106, <https://doi.org/10.1021/cr020529>, 2006.
- Barrett, P. A., Abel, S. J., Coe, H., Crawford, I., Dobracki, A., Haywood, J., Howell, S., Jones, A., Langridge, J., McFarquhar, G. M., Nott, G. J., Price, H., Redemann, J., Shinozuka, Y., Szpek, K., Taylor, J. W., Wood, R., Wu, H., Zuidema, P., ... Zhang, J.: Intercomparison of airborne and surface-based measurements during the CLARIFY, ORACLES and LASIC field experiments, *Atmos. Meas. Tech.*, 15, 6329–6371. <https://doi.org/10.5194/amt-15-6329-2022>, 2022.



- Bates, T. S., Lamb, B. K., Guenther, A., Dignon, J., and Stoiber, R. E.: Sulfur emissions to the atmosphere from natural sources, *J. Atmos. Chem.*, 14, 1–4, <https://doi.org/10.1007/BF00115242>, 1992.
- Brooks, S. D., and Thornton, D. C. O.: Marine aerosols and clouds, *Ann. Rev. Mar. Sci.*, 10, <https://doi.org/10.1146/annurev-marine-121916-063148>, 2018.
- Burkholder, J. B., Sander, S. P., Abbatt, J., Barker, J. R., Huie, R. E., Kolb, C. E., Kurylo, M. J., Orkin, V. L., Wilmouth, D. M., and Wine, P. H.: Chemical Kinetics and Photochemical Data for Use in Atmospheric Studies, Evaluation No. 18, JPL Publication 15-10, Jet Propulsion Laboratory, Pasadena, available at: <http://jpldataeval.jpl.nasa.gov> (last access: 10 May 2024), 2015.
- Burrows, S. M., Easter, R. C., Liu, X., Ma, P. L., Wang, H., Elliott, S. M., Singh, B., Zhang, K., and Rasch, P. J.: OCEANFILMS (Organic Compounds from Ecosystems to Aerosols: Natural Films and Interfaces via Langmuir Molecular Surfactants) sea spray organic aerosol emissions - implementation in a global climate model and impacts on clouds, *Atmos. Chem. Phys.*, 22, <https://doi.org/10.5194/acp-22-5223-2022>, 2022.
- Carshaw, K. S., Lee, L. A., Reddington, C. L., Pringle, K. J., Rap, A., Forster, P. M., Mann, G. W., Spracklen, D. V., Woodhouse, M. T., Regayre, L. A., and Pierce, J. R.: Large contribution of natural aerosols to uncertainty in indirect forcing, *Nature*, 503, <https://doi.org/10.1038/nature12674>, 2013.
- Chen, H., Ezell, M. J., Arquero, K. D., Varner, M. E., Dawson, M. L., Gerber, R. B., and Finlayson-Pitts, B. J.: New particle formation and growth from methanesulfonic acid, trimethylamine and water, *Phys. Chem. Chem. Phys.*, 17, <https://doi.org/10.1039/c5cp00838g>, 2015.
- Chen, Q., Sherwen, T., Evans, M., and Alexander, B.: DMS oxidation and sulfur aerosol formation in the marine troposphere: A focus on reactive halogen and multiphase chemistry, *Atmos. Chem. Phys.*, 18, <https://doi.org/10.5194/acp-18-13617-2018>, 2018.
- Chen, Y. C., Christensen, M. W., Stephens, G. L., and Seinfeld, J. H.: Satellite-based estimate of global aerosol-cloud radiative forcing by marine warm clouds, *Nat. Geosci.*, 7, <https://doi.org/10.1038/ngeo2214>, 2014.
- Chin, M., Jacob, D. J., Gardner, G. M., Foreman-Fowler, M. S., Spiro, P. A., and Savoie, D. L.: A global three-dimensional model of tropospheric sulfate, *J. Geophys. Res.*, 101, <https://doi.org/10.1029/96jd01221>, 1996.
- Croft, B., Martin, R. V., Moore, R. H., Ziemba, L. D., Crosbie, E. C., Liu, H., Russell, L. M., Saliba, G., Wisthaler, A., Müller, M., Schiller, A., Galí, M., Chang, R. Y. W., McDuffie, E. E., Bilsback, K. R., and Pierce, J. R.: Factors controlling marine aerosol size distributions and their climate effects over the northwest Atlantic Ocean region, *Atmos. Chem. Phys.*, 21, <https://doi.org/10.5194/acp-21-1889-2021>, 2021.
- Darmenov, A., and da Silva, A. M.: The Quick Fire Emissions Dataset (QFED) - Documentation of versions 2.1, 2.2 and 2.4. NASA Tech. Rep. Ser. Glob. Model. Data Assim. NASA TM-2013-104606, 32, 1–183, 2013.
- Das, S., Harshvardhan, H., Bian, H., Chin, M., Curci, G., Protonotariou, A. P., Mielonen, T., Zhang, K., Wang, H., and Liu, X.: Biomass burning aerosol transport and vertical distribution over the South African-Atlantic region, *J. Geophys. Res.*, 122, <https://doi.org/10.1002/2016JD026421>, 2017.
- Diamond, M. S., Dobracki, A., Freitag, S., Griswold, J. D. S., Heikkilä, A., Howell, S. G., Kacarab, M. E., Podolske, J. R., Saide, P. E., and Wood, R.: Time-dependent entrainment of smoke presents an observational challenge for assessing aerosol-cloud interactions over the southeast Atlantic Ocean, *Atmos. Chem. Phys.*, 18, <https://doi.org/10.5194/acp-18-14623-2018>, 2018.
- Doherty, S. J., Saide, P. E., Zuidema, P., Shinozuka, Y., Ferrada, G. A., Gordon, H., Mallet, M., Meyer, K., Painemal, D., Howell, S. G., Freitag, S., Dobracki, A., Podolske, J. R., Burton, S. P., Ferrare, R. A., Howes, C., Nabat, P., Carmichael, G. R., Da Silva, A., ... Redemann, J.: Modeled and observed properties related to the direct aerosol radiative effect of biomass burning aerosol over the southeastern Atlantic, *Atmos. Chem. Phys.*, 22, <https://doi.org/10.5194/acp-22-1-2022>, 2022.



- Duncan Fairlie, T., Jacob, D. J., and Park, R. J.: The impact of transpacific transport of mineral dust in the United States, *Atmos. Environ.*, 41, <https://doi.org/10.1016/j.atmosenv.2006.09.048>, 2007.
- Falouna, I.: Sulfur processing in the marine atmospheric boundary layer: A review and critical assessment of modeling uncertainties, *Atmos. Environ.*, 43, <https://doi.org/10.1016/j.atmosenv.2009.02.043>, 2009.
- Formenti, P., Piketh, S. J., and Annegarn, H. J.: Detection of non-sea salt sulphate aerosol at a remote coastal site in South Africa: a PIXE study, *Nucl. Instr. Meth. Phys. Res. B*, 150, 332–338, [https://doi.org/10.1016/S0168-583X\(98\)01041-6](https://doi.org/10.1016/S0168-583X(98)01041-6), 1999.
- Formenti, P., D’Anna, B., Flamant, C., Mallet, M., Piketh, S. J., Schepanski, K., Waquet, F., Auriol, F., Brogniez, G., Burnet, F., Chaboureaud, J. P., Chauvigné, A., Chazette, P., Denjean, C., Desboeufs, K., Doussin, J. F., Elguindi, N., Feuerstein, S., Gaetani, M., ... Holben, B.: The aerosols, radiation and clouds in southern Africa field campaign in Namibia overview, illustrative observations, and way forward, *B. Am. Meteorol. Soc.*, 100, 1277–1298, <https://doi.org/10.1175/BAMS-D-17-0278.1>, 2019.
- Fountoukis, C., and Nenes, A.: ISORROPIA II: a computationally efficient thermodynamic equilibrium model for K^+ - Ca^{2+} - Mg^{2+} - NH_4^+ - Na^+ - SO_4^{2-} - NO_3^- - Cl^- - H_2O aerosols, *Atmos. Chem. Phys.*, 7, 4639–4659, <https://doi.org/10.5194/acp-7-4639-2007>, 2007.
- Galí, M., Levasseur, M., Devred, E., Simó, R., and Babin, M.: Sea-surface dimethylsulfide (DMS) concentration from satellite data at global and regional scales, *BG*, 15, 3497–3519, <https://doi.org/10.5194/bg-15-3497-2018>, 2018.
- Gantt, B., and Meskhidze, N.: The physical and chemical characteristics of marine primary organic aerosol: A review, *Atmos. Chem. Phys.*, 13, 3979–3996, <https://doi.org/10.5194/acp-13-3979-2013>, 2013.
- Gantt, B., Johnson, M. S., Crippa, M., Prévôt, A. S. H., and Meskhidze, N.: Implementing marine organic aerosols into the GEOS-Chem model, *Geosci. Model Dev.*, 8, 619–629, <https://doi.org/10.5194/gmd-8-619-2015>, 2015.
- Gelaro, R., McCarty, W., Suárez, M. J., Todling, R., Molod, A., Takacs, L., Randles, C. A., Darmenov, A., Bosilovich, M. G., Reichle, R., Wargan, K., Coy, L., Cullather, R., Draper, C., Akella, S., Buchard, V., Conaty, A., da Silva, A. M., Gu, W., ... Zhao, B.: The modern-era retrospective analysis for research and applications, version 2 (MERRA-2), *J. Climate*, 30, 5419–5454, <https://doi.org/10.1175/JCLI-D-16-0758.1>, 2017.
- Ghahreman, R., Gong, W., Galí, M., Norman, A. L., Beagley, S. R., Akingunola, A., Zheng, Q., Lupu, A., Lizotte, M., Levasseur, M., and Richard Leitch, W.: Dimethyl sulfide and its role in aerosol formation and growth in the Arctic summer - A modelling study, *Atmos. Chem. Phys.*, 19, <https://doi.org/10.5194/acp-19-14455-2019>, 2019.
- Giles, D. M., Sinyuk, A., Sorokin, M. G., Schafer, J. S., Smirnov, A., Slutsker, I., Eck, T. F., Holben, B. N., Lewis, J. R., Campbell, J. R., Welton, E. J., Korkin, S. V., and Lyapustin, A. I.: Advancements in the Aerosol Robotic Network (AERONET) Version 3 database - Automated near-real-time quality control algorithm with improved cloud screening for Sun photometer aerosol optical depth (AOD) measurements, *Atmos. Meas. Tech.*, 12, 169–209, <https://doi.org/10.5194/amt-12-169-2019>, 2019.
- Haywood, J. M., Abel, S. J., Barrett, P. A., Bellouin, N., Blyth, A., Bower, K. N., Brooks, M., Carslaw, K., Che, H., Coe, H., Cotterell, M. I., Crawford, I., Cui, Z., Davies, N., Dingley, B., Field, P., Formenti, P., Gordon, H., De Graaf, M., ... Zuidema, P.: The CLOUD-Aerosol-Radiation Interaction and Forcing: Year 2017 (CLARIFY-2017) measurement campaign, *Atmos. Chem. Phys.*, 21, <https://doi.org/10.5194/acp-21-1049-2021>, 2021.
- Hodzic, A., Campuzano-Jost, P., Bian, H., Chin, M., Colarco, P. R., Day, D. A., Froyd, K. D., Heinold, B., Jo, D. S., Katich, J. M., Kodros, J. K., Nault, B. A., Pierce, J. R., Ray, E., Schacht, J., Schill, G. P., Schroder, J. C., Schwarz, J. P., Sueper, D. T., ... Jimenez, J. L.: Characterization of organic aerosol across the global remote troposphere: A comparison of ATom measurements and global chemistry models, *Atmos. Chem. Phys.*, 20, <https://doi.org/10.5194/acp-20-4607-2020>, 2020.



- Hoesly, R. M., Smith, S. J., Feng, L., Klimont, Z., Janssens-Maenhout, G., Pitkanen, T., Seibert, J. J., Vu, L., Andres, R. J., Bolt, R. M., Bond, T. C., Dawidowski, L., Kholod, N., Kurokawa, J. I., Li, M., Liu, L., Lu, Z., Moura, M. C. P., O'Rourke, P. R., and Zhang, Q.: Historical (1750-2014) anthropogenic emissions of reactive gases and aerosols from the Community Emissions Data System (CEDS), *Geosci. Model Dev.*, 11(1), <https://doi.org/10.5194/gmd-11-369-2018>, 2018.
- Hoffmann, E. H., Tilgner, A., Schrödner, R., Bräuer, P., Wolke, R., and Herrmann, H.: An advanced modeling study on the impacts and atmospheric implications of multiphase dimethyl sulfide chemistry, *Proc. Natl. Acad. Sci. USA*, 113, 11776–11781, <https://doi.org/10.1073/pnas.1606320113>, 2016.
- Holben, B. N., Eck, T. F., Slutsker, I., Tanré, D., Buis, J. P., Setzer, A., Vermote, E., Reagan, J. A., Kaufman, Y. J., Nakajima, T., Lavenu, F., Jankowiak, I., and Smirnov, A.: AERONET - A federated instrument network and data archive for aerosol characterization, *Remote Sens. Environ.*, 66, 1–16, [https://doi.org/10.1016/S0034-4257\(98\)00031-5](https://doi.org/10.1016/S0034-4257(98)00031-5), 1998.
- Hutchings, L., van der Lingen, C. D., Shannon, L. J., Crawford, R. J. M., Verheye, H. M. S., Bartholomae, C. H., van der Plas, A. K., Louw, D., Kreiner, A., Ostrowski, M., Fidel, Q., Barlow, R. G., Lamont, T., Coetzee, J., Shillington, F., Veitch, J., Currie, J. C., and Monteiro, P. M. S.: The Benguela Current: An ecosystem of four components, *Prog. Oceanogr.*, 83, <https://doi.org/10.1016/j.pocean.2009.07.046>, 2009.
- Jaeglé, L., Quinn, P. K., Bates, T. S., Alexander, B., and Lin, J. T.: Global distribution of sea salt aerosols: New constraints from in situ and remote sensing observations, *Atmos. Chem. Phys.*, 11, <https://doi.org/10.5194/acp-11-3137-2011>, 2011.
- Jaeglé, L., Shah, V., Thornton, J. A., Lopez-Hilfiker, F. D., Lee, B. H., McDuffie, E. E., Fibiger, D., Brown, S. S., Veres, P., Sparks, T. L., Ebben, C. J., Wooldridge, P. J., Kenagy, H. S., Cohen, R. C., Weinheimer, A. J., Campos, T. L., Montzka, D. D., Digangi, J. P., Wolfe, G. M., ... Weber, R. J.: Nitrogen Oxides Emissions, Chemistry, Deposition, and Export Over the Northeast United States During the WINTER Aircraft Campaign, *J. Geophys. Res. - Atmos.*, 123, <https://doi.org/10.1029/2018JD029133>, 2018.
- Jarre, A., Hutchings, L., Kirkman, S. P., Kreiner, A., Tchupalanga, P. C. M., Kainge, P., Uanivi, U., van der Plas, A. K., Blamey, L. K., Coetzee, J. C., Lamont, T., Samaai, T., Verheye, H. M., Yemane, D. G., Axelsen, B. E., Ostrowski, M., Stenevik, E. K., and Loeng, H.: Synthesis: Climate effects on biodiversity, abundance and distribution of marine organisms in the Benguela, *Fish. Oceanogr.*, 24, <https://doi.org/10.1111/fog.12086>, 2015.
- Kaiser, J. W., Heil, A., Andreae, M. O., Benedetti, A., Chubarova, N., Jones, L., Morcrette, J.-J., Razinger, M., Schultz, M. G., Suttie, M., and van der Werf, G. R.: Biomass burning emissions estimated with a global fire assimilation system based on observed fire radiative power, *BG*, 9, 527–554, <https://doi.org/10.5194/bg-9-527-2012>, 2012.
- Kaufman, Y. J., and Tanré, D.: Effect of variations in super-saturation on the formation of cloud condensation nuclei, *Nature*, 369, 45-48, <https://doi.org/10.1038/369045a0>, 1994.
- Lana, A., Bell, T. G., Simó, R., Vallina, S. M., Ballabrera-Poy, J., Kettle, A. J., Dachs, J., Bopp, L., Saltzman, E. S., Stefels, J., Johnson, J. E., and Liss, P. S.: An updated climatology of surface dimethylsulfide concentrations and emission fluxes in the global ocean, *Global Biogeochem. Cy.*, 25, <https://doi.org/10.1029/2010GB003850>, 2011.
- Latimer, R. N. C., and Martin, R. V.: Interpretation of measured aerosol mass scattering efficiency over North America using a chemical transport model, *Atmos. Chem. Phys.*, 19, <https://doi.org/10.5194/acp-19-2635-2019>, 2019.
- Lee, G., Park, J., Jang, Y., Lee, M., Kim, K. R., Oh, J. R., Kim, D., Yi, H. Il, and Kim, T. Y.: Vertical variability of seawater DMS in the South Pacific Ocean and its implication for atmospheric and surface seawater DMS, *Chemosphere*, 78, 1063-1070, <https://doi.org/10.1016/j.chemosphere.2009.10.054>, 2010.



- Lindesay, J. A., Andreae, M. O., Goldammer, J. G., Harris, G., Annegarn, H. J., Garstang, M., Scholes, R. J., and Van Wilgen, B. W.: International geosphere-biosphere programme/international global atmospheric chemistry SAFARI-92 field experiment: Background and overview, *J. Geophys. Res.*, 101, <https://doi.org/10.1029/96jd01512>, 1996.
- Martínez-Lozano, J. A., Utrillas, M. P., Tena, F., and Cachorro, V. E.: The parameterisation of the atmospheric aerosol optical depth using the Ångström power law, *Sol. Energy*, 63, 303–311, [https://doi.org/10.1016/S0038-092X\(98\)00077-2](https://doi.org/10.1016/S0038-092X(98)00077-2), 1998.
- Marvin, M. R., Palmer, P. I., Yao, F., Latif, M. T., and Khan, M. F.: Uncertainties from biomass burning aerosols in air quality models obscure public health impacts in Southeast Asia, *Atmos. Chem. Phys.*, 24, 3699–3715. <https://doi.org/10.5194/acp-24-3699-2024>, 2024.
- Middlebrook, A. M., Murphy, D. M., and Thomson, D. S.: Observations of organic material in individual marine particles at Cape Grim during the First Aerosol Characterization Experiment (ACE 1), *J. Geophys. Res.*, 103, <https://doi.org/10.1029/97JD03719>, 1998.
- Novak, G. A., Fite, C. H., Holmes, C. D., Veres, P. R., Neuman, J. A., Faloona, I., Thornton, J. A., Wolfe, G. M., Vermeuel, M. P., Jernigan, C. M., Peischl, J., Ryerson, T. B., Thompson, C. R., Bourgeois, I., Warneke, C., Gkatzelis, G. I., Coggon, M. M., Sekimoto, K., Bui, T. P., ... Bertram, T. H.: Rapid cloud removal of dimethyl sulfide oxidation products limits SO₂ and cloud condensation nuclei production in the marine atmosphere, *Proc. Natl. Acad. Sci. USA*, 118, <https://doi.org/10.1073/pnas.2110472118>, 2021.
- O'Dowd, C. D., and De Leeuw, G.: Marine aerosol production: A review of the current knowledge, *Phil. Trans. R. Soc. A*, 365, 1753–1774, <https://doi.org/10.1098/rsta.2007.2043>, 2007.
- O'Dowd, C. D., Facchini, M. C., Cavalli, F., Ceburnis, D., Mircea, M., Decesari, S., Fuzzi, S., Young, J. Y., and Putaud, J. P.: Biogenically driven organic contribution to marine aerosol, *Nature*, 431, <https://doi.org/10.1038/nature02959>, 2004.
- Oppo, C., Bellandi, S., Degli Innocenti, N., Stortini, A. M., Loglio, G., Schiavuta, E., and Cini, R.: Surfactant components of marine organic matter as agents for biogeochemical fractionation and pollutant transport via marine aerosols, *Mar. Chem.*, 63, 235–253, [https://doi.org/10.1016/S0304-4203\(98\)00065-6](https://doi.org/10.1016/S0304-4203(98)00065-6), 1999.
- Pai, S. J., Heald, C. L., Pierce, J. R., Farina, S. C., Marais, E. A., Jimenez, J. L., Campuzano-Jost, P., Nault, B. A., Middlebrook, A. M., Coe, H., Shilling, J. E., Bahreini, R., Dingle, J. H., and Vu, K.: An evaluation of global organic aerosol schemes using airborne observations, *Atmos. Chem. Phys.*, 20, <https://doi.org/10.5194/acp-20-2637-2020>, 2020.
- Park, R. J., Jacob, D. J., Chin, M., and Martin, R. V.: Sources of carbonaceous aerosols over the United States and implications for natural visibility, *J. Geophys. Res.*, 108, <https://doi.org/10.1029/2002jd003190>, 2003.
- Philip, S., Martin, R. V., and Keller, C. A.: Sensitivity of chemistry-transport model simulations to the duration of chemical and transport operators: A case study with GEOS-Chem v10-01, *Geosci. Model Dev.*, 9, <https://doi.org/10.5194/gmd-9-1683-2016>, 2016.
- Philip, S., Martin, R. V., Snider, G., Weagle, C. L., Van Donkelaar, A., Brauer, M., Henze, D. K., Klimont, Z., Venkataraman, C., Guttikunda, S. K., and Zhang, Q.: Anthropogenic fugitive, combustion and industrial dust is a significant, underrepresented fine particulate matter source in global atmospheric models, *Environ. Res. Lett.*, 12, 044018, <https://doi.org/10.1088/1748-9326/aa65a4>, 2017.
- Prather, K. A., Bertram, T. H., Grassian, V. H., Deane, G. B., Stokes, M. D., DeMott, P. J., Aluwihare, L. I., Palenik, B. P., Azam, F., Seinfeld, J. H., Moffet, R. C., Molina, M. J., Cappa, C. D., Geiger, F. M., Roberts, G. C., Russell, L. M., Ault, A. P., Baltrusaitis, J., Collins, D. B., ... Zhao, D.: Bringing the ocean into the laboratory to probe the chemical complexity of sea spray aerosol, *Proc. Natl. Acad. Sci. USA*, 110, <https://doi.org/10.1073/pnas.1300262110>, 2013.



- Quinn, P. K., and Bates, T. S. (2011).: The case against climate regulation via oceanic phytoplankton sulphur emissions, *Nature*, 480, 51–56, <https://doi.org/10.1038/nature10580>, 2011.
- Quinn, P. K., Coffman, D. J., Johnson, J. E., Upchurch, L. M., and Bates, T. S.: Small fraction of marine cloud condensation nuclei made up of sea spray aerosol, *Nat. Geosci.*, 10, <https://doi.org/10.1038/ngeo3003>, 2017.
- Ravishankara, A. R., Rudich, Y., Talukdar, R., and Barone, S. B.: Oxidation of atmospheric reduced sulphur compounds: Perspective from laboratory studies, *Philos. T. Roy. Soc. Lond. B.*, 352, 171–182, <https://doi.org/10.1098/rstb.1997.0012>, 1997.
- Redemann, J., Wood, R., Zuidema, P., Doherty, S. J., Luna, B., LeBlanc, S. E., Diamond, M. S., Shinozuka, Y., Chang, I. Y., Ueyama, R., Pfister, L., Ryoo, J. M., Dobracki, A. N., da Silva, A. M., Longo, K. M., Kacenenbogen, M. S., Flynn, C. J., Pistone, K., Knox, N. M., ... Gao, L.: An overview of the ORACLES (ObseRvations of aerosols above CLouds and their intEractionS) project: Aerosol-cloud-radiation interactions in the southeast Atlantic basin, *Atmos. Chem. Phys.*, 21, 1507–1563, <https://doi.org/10.5194/acp-21-1507-2021>, 2021.
- Russell, L. M., Hawkins, L. N., Frossard, A. A., Quinn, P. K., and Bates, T. S.: Carbohydrate-like composition of submicron atmospheric particles and their production from ocean bubble bursting, *Proc. Natl. Acad. Sci. USA*, 107, <https://doi.org/10.1073/pnas.0908905107>, 2010.
- Ryoo, J. M., Pfister, L., Ueyama, R., Zuidema, P., Wood, R., Chang, I., and Redemann, J.: A meteorological overview of the ORACLES (ObseRvations of Aerosols above CLouds and their intEractionS) campaign over the southeastern Atlantic during 2016–2018: Part 1 – Climatology, *Atmos. Chem. Phys.*, 21, 16689–16707, <https://doi.org/10.5194/acp-21-16689-2021>, 2021.
- Seinfeld, J.H. and Pandis, S.N.: *Atmos. Chem. Phys.: From Air Pollution to Climate Change*. John Wiley and Sons, Hoboken, 2016.
- Shannon, L. V., and Nelson, G.: The Benguela: Large Scale Features and Processes and System Variability, in: *The South Atlantic*, Springer, Berlin, Heidelberg, Germany, https://doi.org/10.1007/978-3-642-80353-6_9, 1996.
- Spracklen, D. V., Carslaw, K. S., Kulmala, M., Kerminen, V. M., Sihto, S. L., Riipinen, I., Merikanto, J., Mann, G. W., Chipperfield, M. P., Wiedensohler, A., Birmili, W., and Lihavainen, H.: Contribution of particle formation to global cloud condensation nuclei concentrations, *Geophys. Res. Lett.*, 35, <https://doi.org/10.1029/2007GL033038>, 2008.
- Stier, P., Schutgens, N. A. J., Bellouin, N., Bian, H., Boucher, O., Chin, M., Ghan, S., Huneeus, N., Kinne, S., Lin, G., Ma, X., Myhre, G., Penner, J. E., Randles, C. A., Samset, B., Schulz, M., Takemura, T., Yu, F., Yu, H., and Zhou, C.: Host model uncertainties in aerosol radiative forcing estimates: Results from the AeroCom Prescribed intercomparison study, *Atmos. Chem. Phys.*, 13, <https://doi.org/10.5194/acp-13-3245-2013>, 2013.
- Su, M., Shi, Y., Yang, Y., and Guo, W.: Impacts of different biomass burning emission inventories: Simulations of atmospheric CO₂ concentrations based on GEOS-Chem, *Sci. Total Environ.*, 876, <https://doi.org/10.1016/j.scitotenv.2023.162825>, 2023.
- Swap, R., Garstang, M., Macko, S. A., Tyson, P. D., Maenhaut, W., Artaxo, P., Källberg, P., and Talbot, R.: The long-range transport of southern African aerosols to the tropical South Atlantic, *J. Geophys. Res.*, 101, <https://doi.org/10.1029/95jd01049>, 1996.
- Swap, R. J., Annegarn, H. J., Suttles, J. T., King, M. D., Platnick, S., Privette, J. L., and Scholes, R. J.: Africa burning: A thematic analysis of the Southern African Regional Science Initiative (SAFARI 2000), *J. Geophys. Res.-Atmos.*, 108, <https://doi.org/10.1029/2003jd003747>, 2003.
- Tashmim, L., Porter, W. C., Chen, Q., Alexander, B., Fite, C. H., Holmes, C. D., Pierce, J. R., Croft, B., and Ishino, S.: Contribution of expanded marine sulfur chemistry to the seasonal variability of dimethyl sulfide oxidation



products and size-resolved sulfate aerosol, *Atmos. Chem. Phys.*, 24, <https://doi.org/10.5194/acp-24-3379-2024>, 2024.

Tournadre, J.: Anthropogenic pressure on the open ocean: The growth of ship traffic revealed by altimeter data analysis, *Geophys. Res. Lett.*, 41, <https://doi.org/10.1002/2014GL061786>, 2014.

Van Der Werf, G. R., Randerson, J. T., Giglio, L., Collatz, G. J., Mu, M., Kasibhatla, P. S., Morton, D. C., Defries, R. S., Jin, Y., and Van Leeuwen, T. T.: Global fire emissions and the contribution of deforestation, savanna, forest, agricultural, and peat fires (1997-2009), *Atmos. Chem. Phys.*, 10, <https://doi.org/10.5194/acp-10-11707-2010>, 2010.

Van Der Werf, G. R., Randerson, J. T., Giglio, L., Van Leeuwen, T. T., Chen, Y., Rogers, B. M., Mu, M., Van Marle, M. J. E., Morton, D. C., Collatz, G. J., Yokelson, R. J., and Kasibhatla, P. S.: Global fire emissions estimates during 1997-2016, *Earth Syst. Sci. Data*, 9, 697–720, <https://doi.org/10.5194/essd-9-697-2017>, 2017.

Veres, P. R., Andrew Neuman, J., Bertram, T. H., Assaf, E., Wolfe, G. M., Williamson, C. J., Weinzierl, B., Tilmes, S., Thompson, C. R., Thames, A. B., Schroder, J. C., Saiz-Lopez, A., Rollins, A. W., Roberts, J. M., Price, D., Peischl, J., Nault, B. A., Möller, K. H., Miller, D. O., ... Ryerson, T. B.: Global airborne sampling reveals a previously unobserved dimethyl sulfide oxidation mechanism in the marine atmosphere, *Proc. Natl. Acad. Sci. USA*, 117, <https://doi.org/10.1073/pnas.1919344117>, 2020.

Vignati, E., De Leeuw, G., and Berkowicz, R.: Modeling coastal aerosol transport and effects of surf-produced aerosols on processes in the marine atmospheric boundary layer, *J. Geophys. Res.*, 106, <https://doi.org/10.1029/2000JD000025>, 2001.

Wang, X., Heald, C. L., Ridley, D. A., Schwarz, J. P., Spackman, J. R., Perring, A. E., Coe, H., Liu, D., and Clarke, A. D.: Exploiting simultaneous observational constraints on mass and absorption to estimate the global direct radiative forcing of black carbon and brown carbon, *Atmos. Chem. Phys.*, 14, <https://doi.org/10.5194/acp-14-10989-2014>, 2014.

Wizenberg, T., Strong, K., Jones, D. B. A., Lutsch, E., Mahieu, E., Franco, B., and Clarisse, L.: Exceptional wildfire enhancements of PAN, C₂H₄, CH₃OH, and HCOOH over the Canadian high Arctic during August 2017, *J. Geophys. Res.-Atmos.*, 128, <https://doi.org/10.1029/2022JD038052>, 2023.

Wood, R.: Stratocumulus clouds, *Mon. Weather Rev.*, 140, 2373–2423, <https://doi.org/10.1175/MWR-D-11-00121.1>, 2012.

Wu, R., Wang, S., and Wang, L.: New mechanism for the atmospheric oxidation of dimethyl sulfide. The importance of intramolecular hydrogen shift in a CH₃SCH₂O radical, *J. Phys. Chem. A*, 119, 112–117, <https://doi.org/10.1021/jp511616j>, 2015.

Yu, F., Luo, G., and Ma, X.: Regional and global modeling of aerosol optical properties with a size, composition, and mixing state resolved particle microphysics model, *Atmos. Chem. Phys.*, 12, <https://doi.org/10.5194/acp-12-5719-2012>, 2012.

Zhai, S., Jacob, D. J., Brewer, J. F., Li, K., Moch, J. M., Kim, J., Lee, S., Lim, H., Lee, H. C., Kuk, S. K., Park, R. J., Jeong, J. I., Wang, X., Liu, P., Luo, G., Yu, F., Meng, J., Martin, R. V., Travis, K. R., ... Liao, H.: Relating geostationary satellite measurements of aerosol optical depth (AOD) over East Asia to fine particulate matter (PM_{2.5}): insights from the KORUS-AQ aircraft campaign and GEOS-Chem model simulations, *Atmos. Chem. Phys.*, 21, <https://doi.org/10.5194/acp-21-16775-2021>, 2021.

Zuidema, P., Redemann, J., Haywood, J., Wood, R., Piketh, S., Hipondoka, M., and Formenti, P.: Smoke and clouds above the southeast Atlantic: Upcoming field campaigns probe absorbing aerosol's impact on climate, *B. Am. Meteorol. Soc.*, 97, 1131–1135, <https://doi.org/10.1175/BAMS-D-15-00082.1>, 2016.